Energy Reports 7 (2021) 8421–8446

Contents lists available at ScienceDirect

Energy Reports

journal homepage: www.elsevier.com/locate/egyr

Review article

# Recent development of hydrogen and fuel cell technologies: A review

Lixin Fan [a], Zhengkai Tu [a,*], Siew Hwa Chan [b]

[a] School of Energy and Power Engineering, Huazhong University of Science and Technology, Wuhan, 430074, China
[b] Energy Research Institute at Nanyang Technological University (ERI@N), 50 Nanyang Avenue, Singapore 639798, Singapore

ARTICLE INFO

*Article history:*
Received 26 June 2020
Received in revised form 30 June 2021
Accepted 2 August 2021
Available online 27 August 2021

*Keywords:*
Fuel cell
Hydrogen technology
Fuel cell vehicles
Membrane electrode assembly
Hydrogen strategy

ABSTRACT

Hydrogen has emerged as a new energy vector beyond its usual role as an industrial feedstock, primarily for the production of ammonia, methanol, and petroleum refining. In addition to environmental sustainability issues, energy-scarce developed countries, such as Japan and Korea, are also facing an energy security issue, and hydrogen or hydrogen carriers, such as ammonia and methylcyclohexane, seem to be options to address these long-term energy availability issues. China has been eagerly developing renewable energy and hydrogen infrastructure to meet their sustainability goals and the growing energy demand. In this review, we focus on hydrogen electrification through proton-exchange membrane fuel cells (PEMFCs), which are widely believed to be commercially suitable for automotive applications, particularly for vehicles requiring minimal hydrogen infrastructure support, such as fleets of taxies, buses, and logistic vehicles. This review covers all the key components of PEMFCs, thermal and water management, and related characterization techniques. A special consideration of PEMFCs in automotive applications is the highlight of this work, leading to the infrastructure development for hydrogen generation, storage, and transportation. Furthermore, national strategies toward the use of hydrogen are reviewed, thereby setting the rationale for the hydrogen economy.



**Contents**



* Corresponding author.
*E-mail address:* tzklq@hust.edu.cn (Z. Tu).

https://doi.org/10.1016/j.egyr.2021.08.003

## 1. Introduction

Safe, environmentally friendly, and reliable energy supplies are essential to mankind for sustainability and a high quality of life, although their provision is subjected to social, political, environmental, and economic challenges. It is generally acknowledged that there is no single energy source that can dominate and govern the global energy market, and thus an energy-mix model has been widely accepted, which benefits from the availability of usable resources in each country/region or the choice of importing energy resources. Hydrogen, a clean energy carrier, is the most abundant chemical element in the universe, accounting for 75% of normal matter by mass and over 90% by number of atoms. When hydrogen gas is oxidized electrochemically in a fuel cell system, it generates pure water as a by-product, emitting no carbon dioxide. Hydrogen has emerged as a new energy vector beyond its usual role as an industrial feedstock, primarily for the production of ammonia, methanol, and petroleum refining. There are expanding applications for hydrogen to be used in many other fields, like transportation, power generation, and militarized equipment for its advantages of high efficiency and low emission.

The rapid development of hydrogen technology and growing energy needs drive many countries to set domestic hydrogen roadmap. It is obvious that hydrogen and fuel cells can meet the rising demands for societal development and provide the possibility of covering most energy fields. Therefore, many countries include hydrogen development in their national strategies and implement measures to promote the fuel cell industry. For example, in Japan, the government has elevated hydrogen energy to a national strategy, including a mature industrial chain leading in technology and commercialization, with a production capacity of over 10,000 units of Toyota Mirai, more than 300,000 sets of Ene-farm cogeneration systems, and more than 100 HRS (Oh et al., 2008; Wang et al., 2020).

The strategic energy roadmaps of Korea (Anon, 2018b), Japan (Anon, 2017), China (Anon, 2015a), and Europe (Anon, 2019) are depicted in Figs. 1–4. Among these roadmaps, high efficiency, stability, low carbon emission, low cost and scale production are the same developing goals. Apart from environmental sustainability, energy-scarce developed countries, such as Japan, Korea, and Singapore, are also facing energy security issues, and hydrogen seem to be options to address long-term energy availability issues. Japan has addressed a full and detailed roadmap for hydrogen production, stationary fuel cell, fuel cell vehicles (FCVs), and commercial applications from 2020 to 2030. Developing nations, such as China, are also actively developing renewable energy and hydrogen infrastructure, especially FCVs and hydrogen refuel stations (HRS), to meet their sustainability goals, as well as the growing energy demand.

In this review, we focus on hydrogen electrification through proton-exchange membrane fuel cells (PEMFCs), which are widely believed to be commercially ready for automotive applications, particularly for those vehicles that require minimum hydrogen infrastructure support, such as fleets of taxies, buses, and logistic vehicles. Meanwhile, this review covers the key components of PEMFCs, thermal and water management in membrane-electrode assemblies (MEAs), and where appropriate, the advanced characterization techniques applied. A special consideration of PEMFCs in automotive applications is the highlight of this work, which leads to the infrastructure development for hydrogen generation, storage, and transportation. In addition, policy support, global targets, and challenges are observed to demonstrate the worldwide attitude to hydrogen and fuel cells. Finally, downstream applications of hydrogen other than those in the automotive sector are briefly reviewed, thereby setting the rationale for the hydrogen economy.

## 2. Fuel cells

A fuel cell is an energy conversion device that continuously converts chemical energy in a fuel into electrical energy, as long as both the fuel and oxidant are available. It exhibits advantageous characteristics exceeding conventional combustion-based technologies that are currently applied in certain critical fields, such as electronic, housing power, power plants, passenger vehicles, as well as military applications. Operating with higher efficiency than combustion engines, fuel cells demonstrate an electrical energy conversion efficiency of 60% or more, with lower emissions. Water is the only product of the power generation process in hydrogen fuel cells, and thus there are no carbon dioxide emissions or air pollutants that create smog and cause health problems during operation. Moreover, fuel cells emit low noise during operation, because they contain fewer moving parts. Fuel cells come in many varieties, but they all work in generally the same manner. In essence, a fuel cell consists of three adjacent segments, namely, the anode, electrolyte, and cathode. When hydrogen undergoes an oxidation reaction at the anode ($H_2 \rightarrow 2H^+ + 2e^-$), it generates cations that migrate to the cathode through the electrolyte and free electrons that flow the external circuit. Contrarily, a reduction reaction occurs at the cathode, where oxygen is reduced to water by the cations and electrons (Ralph et al., 1998). The electrochemical reaction that occurs at the cathode is $4H^+ + O^2 + 4e^- \rightarrow 4H_2O$. Based on the type of electrolyte used, fuel cells can be categorized into alkaline fuel cells (AFCs), PEMFCs, phosphoric acid fuel cells (PAFCs), molten carbonate fuel cells (MCFCs), and solid oxide fuel cells (SOFCs). And the classification and characteristics of fuel cells are listed in Table 1 (Qiang, 2005). The electrolytes of AFCs are KOH with $OH^-$ serving as mobile ions under lower oxygen reduction overpotential and lower operating temperature (20∼80 °C). The mobile ions of PEMFCs are $H^+$ with the operating temperature from −40 °C to 90 °C, air and oxygen can be the oxidants in the cathode. PAFCs and MCFCs are utilized in power station for its large output range. Ceramic materials, like $Y_2O_3$–$ZrO_2$, served as electrolyte during the operation of SOFCs under high temperature (600∼1000 °C). As shown in Fig. 5, fuel cells can be used in different scenes based on the required power output scale. The distinctive advantages of rapid start-up time, wild range operating temperature (−40–90 °C), high specific energy have made PEMFC stand out from all types fuel cell and wildly be used in fuel cell vehicles and stationary applications. The typical structure of a PEMFC is illustrated in Fig. 6 and the detailed explanation of these components and related researches are introduced in following parts. Additionally, water management and thermal management are the key issues of PEMFC, which are introduced in detailed.

### 2.1. Membrane-electrode assembly

MEA is a component including three layers, namely, membrane, gas diffusion layer (GDL), and catalyst layer (CL) to provide microchannels for mass transport and electrochemical reactions, and influence the performance, durability, and cost of

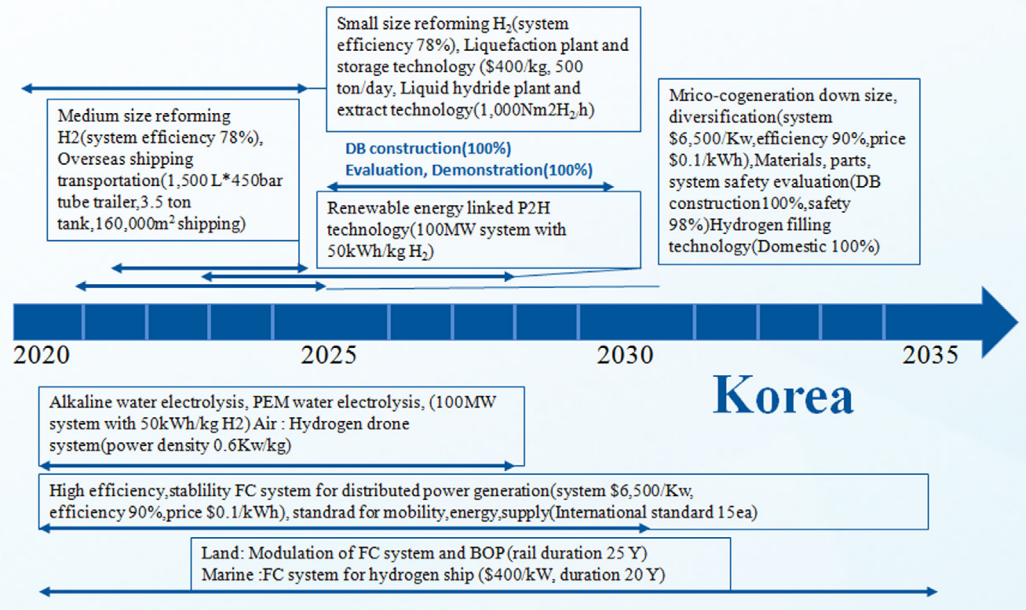


**Fig. 1.** Strategy and roadmap of Korea for hydrogen and fuel cells from 2020 to 2035 (Anon, 2018b).

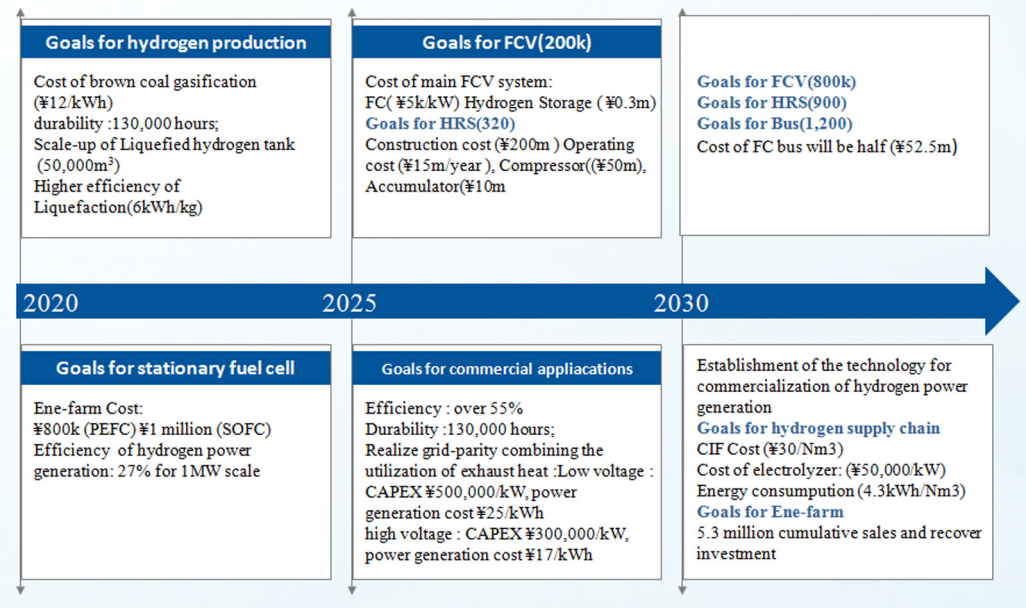


**Fig. 2.** Strategy and roadmap of Japan for hydrogen and fuel cells from 2020 to 2030 (Anon, 2017).

PEMFC (Adamson et al., 2008). The structure of MEA is shown in Fig. 6. GDL provides channels for gas and electrons, supports the CL, conducts electrons, and discharges water generated from the reactions of the PEMFC (Lin et al., 2010). The GDL consists of carbon, water, alcohol, polytetrafluoroethylene (PTFE), or another hydrophobic substance. PTFE is used to promote the transport of gas and water during operation under flooding conditions (Iyuke et al., 2003; Litster and McLean, 2004). The CL is where the electrochemical reaction occurs that converts hydrogen gas and oxygen (in air) into water and electricity. The CL thickness typically varies in the range of 5–100 μm, with a porosity of 40–70%, and the catalyst with a particle size of 1–10 nm should be well dispersed within the CL (Van Dao et al., 2019).

Three generations of MEA have developed with the increasing demand for large-scale commercialization of PEMFCs, significantly improving their performance and lifespan and reducing the cost. They are the gas diffusion electrode (GDE), catalyst-coated membrane (CCM), and oriented MEA. Table 2 presents the Pt loading, minimum electrical resistance, and cost of these three MEA and the DOE 2020 target. Fig. 7 shows the development and fabrication methods of the three generations of MEA. The mature preparation process of the GDE (Hezarjaribi et al., 2014) is easy and simple, involving the coating of a CL on a GDL to form a PEM, and then forming an MEA by hot pressing. However, the amount of catalyst is difficult to control accurately, resulting in low utilization of the catalyst (lower than 20%) and high cost. Companies that specialize in high-volume production of GDE include Johnson Matthey, Gore, and Gaskatel. However, there are many companies that produce custom or low-quantity GDE, enabling different shapes, catalysts, and loadings to be evaluated as well, which include Fuel Cell Store and Fuel Cells Etc. Owing to the different expansion systems of GDL and PEM, it is easy

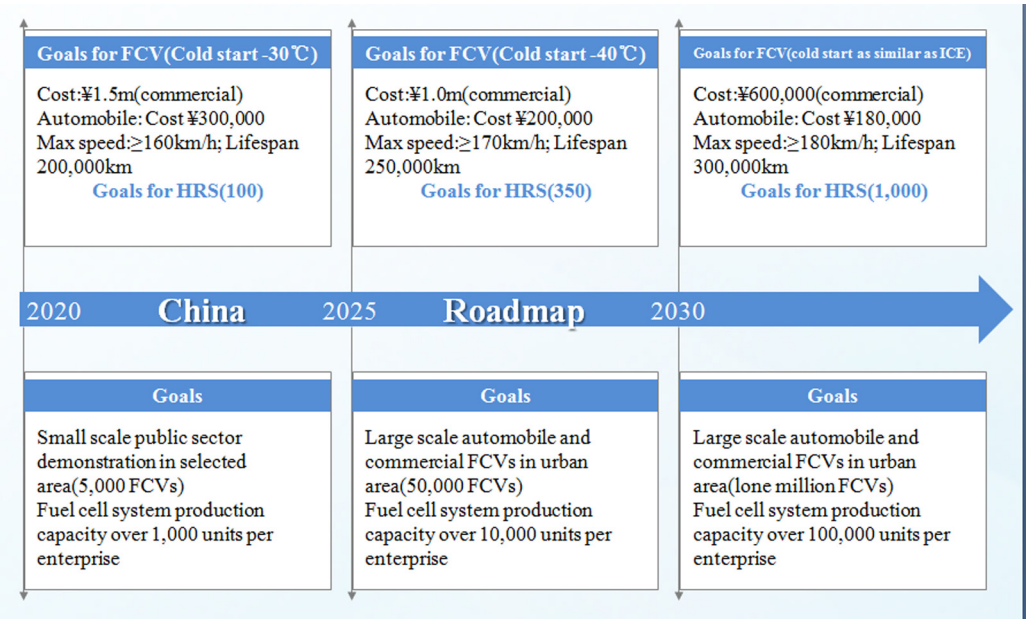


**Fig. 3.** Strategy and roadmap of China for hydrogen and fuel cells from 2020 to 2030 (Anon, 2015a).

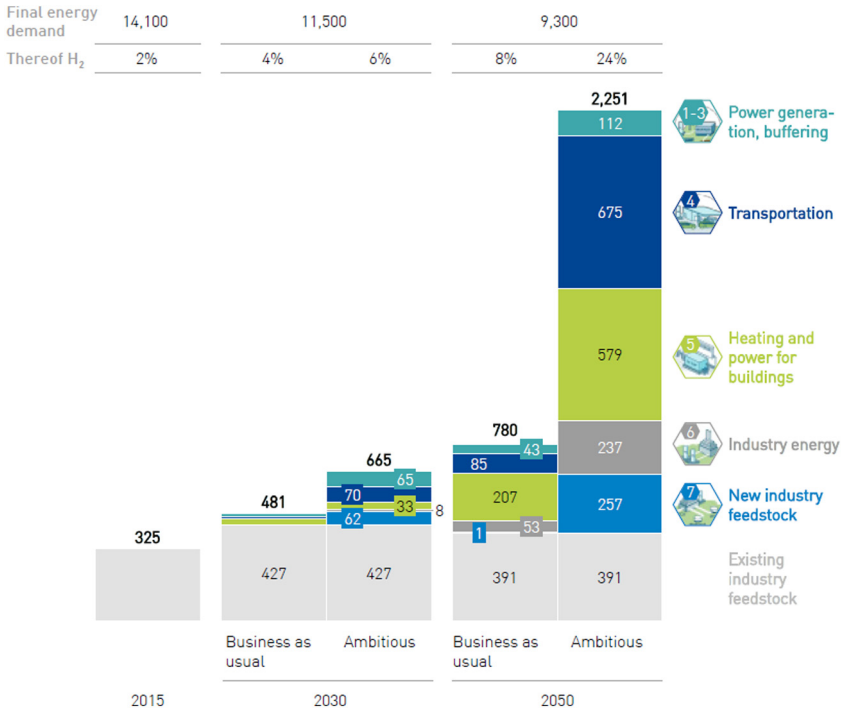


**Fig. 4.** Ambitious scenario for Energy demand and the Hydrogen deployment For Europe from 2015 to 2050 (Anon, 2019).

for part of the interface to be isolated, causing an increase in the internal contact resistance. Therefore, GDE has been nearly abandoned in commercial manufacturing. Ultrasonic spray methods, a technique combining spraying and ultrasonic atomization, are used to prepare CCM by pressing a GDL with two catalyst-coated sides and a PEM into an MEA with evenly dispersing catalyst particles as Fig. 7(b). In this way, the prepared MEA demonstrates a better performance with low resistance, good proton transfer ability, high Pt utilization, and low cost in comparison with the first generation, resulting in its wide application in large-scale commercialization. At present, the main companies providing large-scale MEA manufacturing are 3M, Johnson Matthey, Gore, Toray, Kolon, and Ballard, whereas certain vehicle companies, such as Toyota and Honda, produce MEA only for their own utilization. The latest generation is oriented MEA, which was first proposed in 2002 by Middelman et al. by coating uniform Pt particles (2 μm) and then coating a proton conductor (10 μm) on the surface of oriented carbon (Middelman, 2002). 3M developed a commercial nanostructured thin film (NSTF) by growing whiskers onto a microstructured substrate and then coating Pt on the whiskers with controlled loading though roll-to-roll vacuum sputtering (Debe, 2013). NSTF exhibits higher catalyst utilization, activity, and stability with a thickness of 0.25–0.4 μm (5% of the thickness of traditional Pt/C electrodes) and almost 100% utilization of Pt.

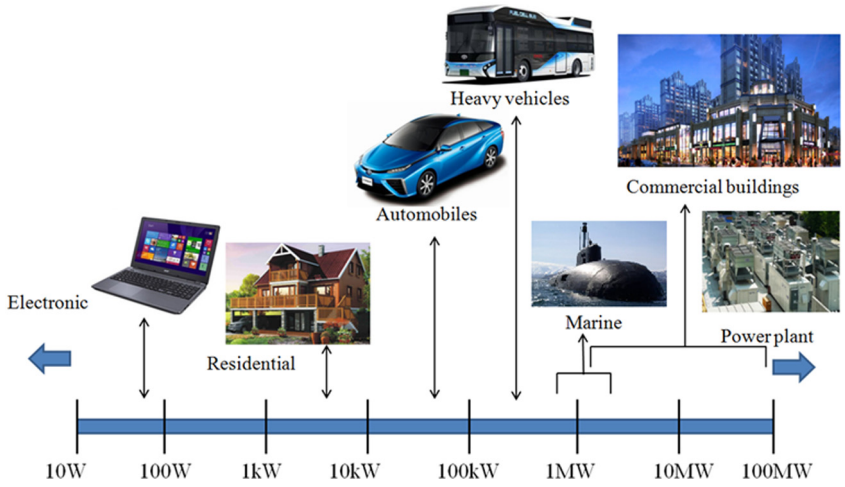


**Fig. 5.** Scheme of some typical applications of fuel cell.

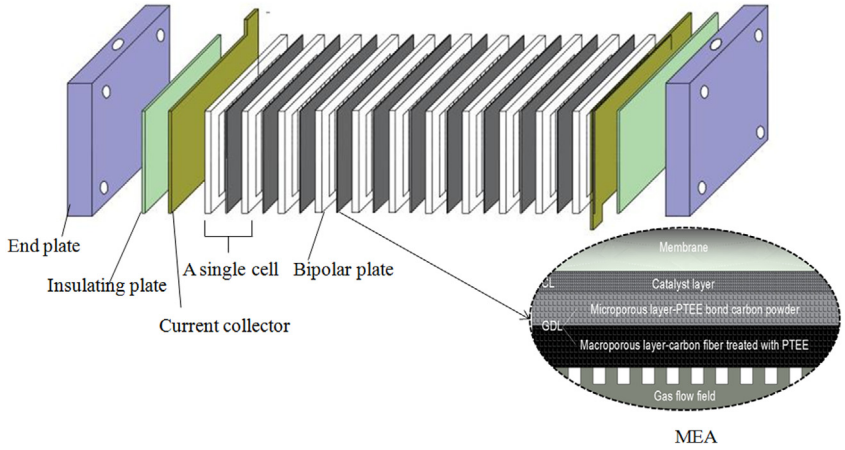


**Fig. 6.** Basic structure of typical integrating PEMFC stack with end plate, insulating plate, current collector, bipolar plate, MEA, and the image of MEA structure.

**Table 1**
Classification and characteristics of fuel cells (Qiang, 2005).

| Type | AFCs | PEMFCs | PAFCs | MCFCs | SOFCs |
|---|---|---|---|---|---|
| Electrolyte | KOH | Perfluorosulfonic acid ionic exchange membrane | $H_3PO_4$ | $Li_2\ CO_3$-$K_2CO_3$ | $Y_2\ O_3$–$ZrO_2$ |
| Conductible ions | $OH^-$ | $H^+$ | $H^+$ | $CO_3^{2-}$ | $O^{2-}$ |
| Fuel | $H_2$ | $H_2$, $CH_3OH$ | Reformed fuel ($CH_4$, CO, $H_2$) | Purified coal gas, natural gas, and reformed fuel ($CH_4$, CO, $H_2$) | Purified coal gas and natural gas ($CH_4$, CO) |
| Oxidant | $O_2$ | Air | Air | Air | Air |
| Catalyst | Pt/Ru | Pt/Ru | Pt | NiO | Ni |
| Operating temperature | 65–220 °C | −40–90 °C | 150–200 °C | 650–700 °C | 600–1000 °C |
| Theoretical voltage | 1.18 V | 1.18 V | 1 V | 1.116 V | 1.13 V |
| System efficiency | 60%–70% | 43%–68% | 40%–55% | 55%–65% | 55%–65% |
| Application | Special ground and aerospace | Electric vehicle, submarine, and mobile power source | Regional power supply (e.g., power plant) | Power station | Power station |
| Development | Rapid development at 1–100 kW | Rapid development at 1–300 kW with high cost | Rapid development at 1–200 kW with high cost | Mainly development at 250–2000 kW with short life | Mainly development at 1–200 kW with high preparation technology cost |

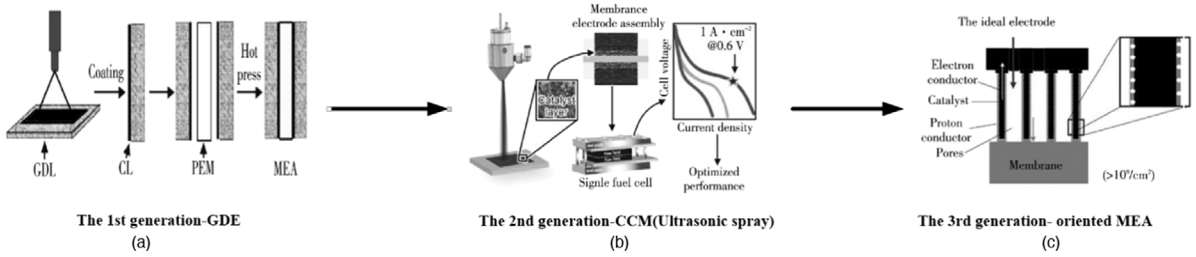


**Fig. 7.** Schemes of three generations of MEA (Hezarjaribi et al., 2014; Debe, 2013; Murata et al., 2014): (a)Hot press applied in GDE fabrication;(b) Schematic of assembling CCM with ultrasonic spray; (c) Structure of oriented MEA by 3M.

Considerable research has been conducted on MEA to improve its performance and lifespan, and Majlan et al. (2018) presented a comprehensive review of electrodes, taking all aspects into consideration, including the function and fabrication process of all components and cell durability. There is an increasing body of research on CL for its distinguished effect on cell performance. The active area and the thickness of CL are influenced by the Pt loading, which in turn affects the mass transfer and water management. Qu et al. (2019) developed a series of MEA with different Pt loading levels and evaluated the degradation of the Pt/C catalyst by scanning electron microscopy (SEM). They concluded that the performance degradation of MEAs could be mitigated by increasing the Pt loading. However, a higher Pt loading would lead to a thicker CL, and hence poorer mass transfer and possibly carbon material corrosion. A Pt/C double-layer catalyst (57.2 $m^2$ $g^{-1}$Pt) was fabricated (Van Dao et al., 2019) to enhance the electrocatalytic properties of electrodes with more Pt active sites than obtained by the electrophoresis deposition method (31.9 $m^2$ $g^{-1}$Pt).

### 2.2. Proton-exchange membrane (PEM)

A PEM has the main functions of conducting protons, separating fuel oxidizer and insulating protons, and its performance directly affects the performance of PEMFCs. An ideal PEM should exhibit a high proton conductivity rate, proper water content and gas molecular permeability, good electrochemical stability and mechanical stability, with ideal characteristics of a decomposition temperature of 250–500 °C, water absorption rate of 2.5–27.5 $H_2O/SO_3H$, and conductivity in the range of $10^{-5}$–$10^{-2}$ S $cm^{-1}$.

Most fuel cells use Nafion membranes manufactured by DuPont, and Fig. 8 shows a general chemical formula for the perfluorosulfonic acid membrane (PFSA) ionomers (Kusoglu and Weber, 2017). The production process of a membrane is relatively complicated, and the current market price is relatively expensive (approximately 2000 $ $m^{-2}$). Reducing production costs and improving chemical and mechanical stabilities are important goals in the development of PEMs. In recent years, with the continuous advancement of Nafion membranes and the development of new membranes, Ballard developed a PFSA membrane with properties comparable to those of Nafion membranes. The production process of such a PFSA membrane is relatively simple and the processing cost is low. If the market demand continues to increase, the cost of the membrane could be significantly reduced by mass production.

Apart from the PFSA membrane, some alternative membranes have been developed. Representative examples include polybenzimidazole (PBI)-based membranes, sulfonated aromatic (such as polyphenylsulfone and SPEEK) membranes, phosphonic-based membranes, polyphosphazene-based membranes (SPE), and polystyrene sulfonic acid (PSSA) membranes (Scofield et al., 2015), and their chemical structures are shown in Fig. 9. Among them, PBI exhibits better chemical and physical properties, with an operating temperature range from 100 to 200 °C, while the temperature range of polyphenylsulfone is up to 230 °C as well as SPE membranes applied in high-temperature PEMFCs. By using the optimum binder content and the same catalyst loading (0.5 mg $cm^{-2}$) and active area (5 $cm^2$), Su et al. (2013) developed five types of GDEs, namely, polyvinylidene fluoride (PVDF), sulfonated polymer (Nafion), PBI, fluorinated ethylene propylene (FEP), and PBI/PVDF. In a single cell, the PTFE and PVDF-based GDEs are considered to be very promising for commercial applications (Fig. 10), having shown the best performance compared with the others. The power and current densities at 0.6 V and 160 °C were 0.61 W $cm^{-2}$ and 0.52 A $cm^{-2}$ respectively, which was over 120% higher than that of PBI and Nafion-based GDEs (0.24 A $cm^{-2}$ under the same conditions). Although many studies have investigated and characterized the influence of hydrophobic materials used in various GDLs, the role of the GDL in the mechanism of the mass transport of the reactants and products has not been clearly discussed, owing to its complicated microstructure, multiphase composition, and multicomponent structure.

There is a promising trend toward developing hybrid membranes on the basis of existing backbones with known functions, so as to achieve a particular function efficiently. Some novel membranes have been created to improve the efficiency under different working requirements. Sutradhar et al. (2019) synthesized a promising membrane, sulfonated poly phenylene benzo phenone membrane (SPPBP), through carbon–carbon coupling polymerization for PEMFCs with the properties of high thermal and chemical stabilities and high proton conductivity (up to 92.90 mS $cm^{-1}$). Moreover, the results demonstrated that SPPBP exhibited an ion exchange capacity of 1.18–2.30 meq $g^{-1}$ and water uptake of 34.2–78.3%. Neethu et al. (2019) investigated a new PEM incorporated with activated carbon extracted from coconut shell (ACGS), which could improve the proton exchange with high porosity and superior specific surface area, and natural clay, which could lower the cost to approximately 45 $ $m^{-2}$. As a result, the ACGS/Clay membrane overcame the drawbacks of organic nature to be degradable though bacteria and exhibited better performance than a Nafion membrane fuel cell, with a higher proton coefficient ($36 \times 10^{-6}$ $cm^2$ $s^{-1}$), 1.5-fold higher operating voltage, and two-fold higher power density. Haragirimana et al. (2019) fabricated a series of four sulfonated poly aryl ether sulfones (SPAES) copolymer blend PEMs with different sulfonation degrees, leading to better thermal and mechanical stabilities, better hydrolytic and oxidative stabilities, and lower methanol permeability than the control membrane. The B4 membrane was experimentally found to exhibit the highest proton conductivity of 203.1 mS $cm^{-1}$ at 90 °C and 169.2 mS $cm^{-1}$ at 94.1% RH, achieving a power density of 467.98 mW $cm^{-2}$ at a current density of 1050 mA $cm^{-2}$ in a PEMFC. Oh et al. (2019) fabricated a Nafion-sulfonated silica acid (Nafion-SSA) composite membrane with better thermal and mechanical stabilities and phase morphology than a Nafion membrane. Owing to the advance of Nafion-SSA, a Nafion-SSA 1.0 wt % composite membrane,

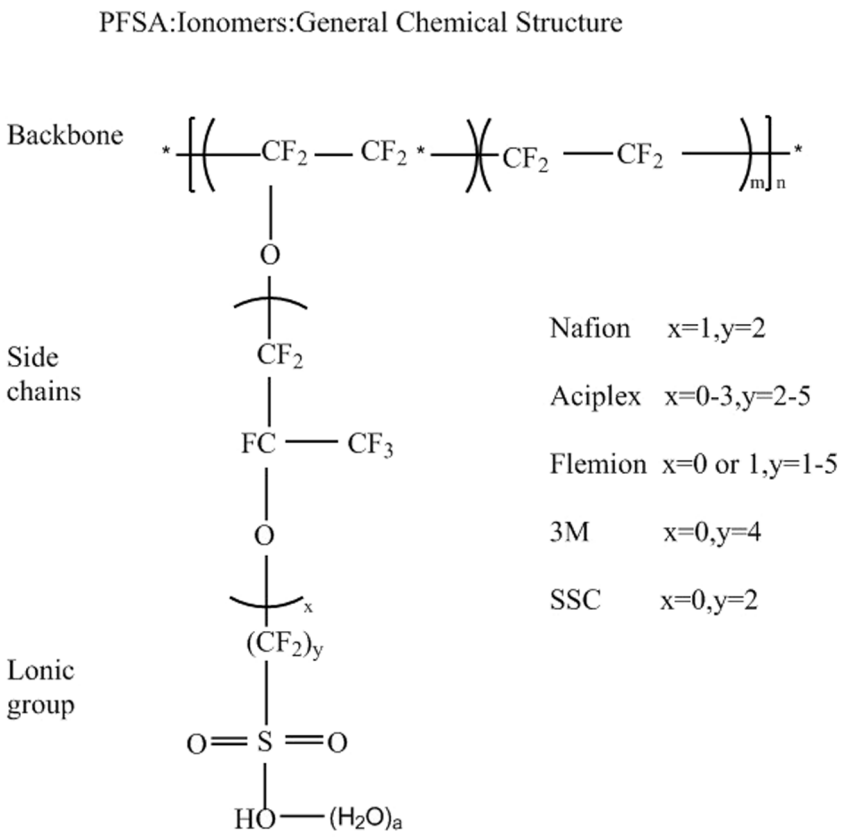


**Fig. 8.** General chemical formula for PFSA ionomers in various forms (Kusoglu and Weber, 2017).

**Table 2**
Property comparison of there generation of MEA and DOE 2020.

| Parameter | Unit | GDE | CCM(Gore) | Oriented MEA(3M) | DOE 2020 |
|---|---|---|---|---|---|
| Pt loading | mg $cm^{-2}$ | 0.4 | 0.2 | 0.147 | 0.125 |
| Minimum Electrical Resistance | Ω $cm^{-2}$ | 7800–12300 | 2000–5600 | 861 | 1000 |
| Cost | \$ $kW^{-1}$ | 35–50 | 17–25 | 7–15 | 20 |

in a completely humid state, showed a proton conductivity twice as high as that of recast Nafion, and achieved maximum power and current densities of 454 mW $cm^{-2}$ and 2026 mA $cm^{-2}$, respectively, which were 2.8 times higher than those of recast Nafion.

Thin-film coating methods have been widely used in fabricating PEMs since their development in 1993; with the subsequent development of fuel cells, optimizing the preparation method of PEM has become one of the main trends of contemporary research. In addition to thin-film methods, traditional preparation methods include vacuum deposition and electrodeposition. Paul et al. (2019) applied hot embossing to create hexagonal cylindrical microstructures of various aspect ratios, to be embedded into MAEs in Nafion membranes. Their results demonstrate that these microstructured PEMs perform better than planar PEMs in hot start-up conditions, but with the observation of a high hydrogen crossover and short-circuit current. Teixeira et al. (2019) used impregnation and casting methods to incorporate a derivative of arylmono acid or bisphosphonic acid into the Nafion membrane, demonstrating that the proton conductivity of the membrane created by casting was 1.55 times higher than that of the regular membrane at 30, 40, and 50 °C. A comparison revealed that bisphosphonic acid dopants exhibited better performance than monophosphonic acid dopants, whereas dopants with a second phosphonic acid group improved the proton conductivity. Wang et al. (2019a) invented a porous nanofiber composite membrane (PNFCM) by impregnating a nanofiber mat, prepared by a hybrid electrospinning and soft template method, with chitosan. The result demonstrated that the PNFCM achieved vertical conductivities of 307 mS $cm^{-1}$ at 90 °C and 100% relative humidity (RH), which was 3.2 times that of a traditional nanofiber composite membrane, as well as the maximum current density of 1818 mA $cm^{-2}$ and power density of 502 mW $cm^{-2}$ at 60 °C and 75% RH.

Overall, there are two main trends in the PEM development process. On the one hand, the thickness of the membrane is reduced from 50–150 nm to 5–25 um owing to the improvement of fabrication methods, resulting in a significant drop in the cell ohmic impedance and intensity at a high current density. On the other hand, the substitutes of PFSA become the highlight of the membrane field in reducing the cost and ensuring safety, resulting in hydrocarbon polymers attracting considerable support for their distinctive characteristics.

### 2.3. Catalyst

Catalysts are the key materials in fuel cells, and their main challenge is the cost of platinum, a noble metal that is widely utilized as a catalyst owing to its good work function and chemical

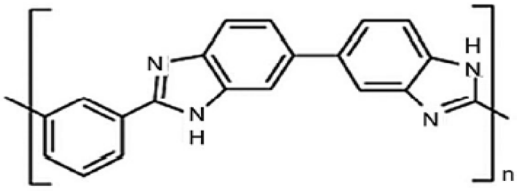

(a)

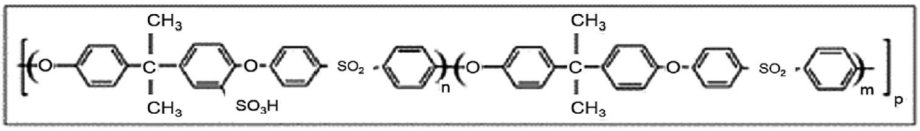

(b)

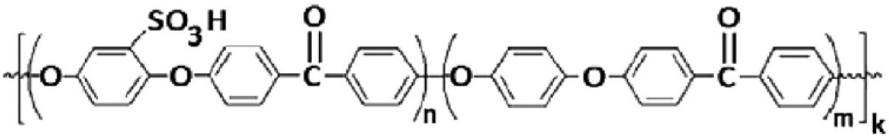

(c)

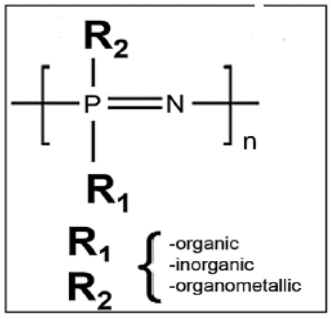


(d)

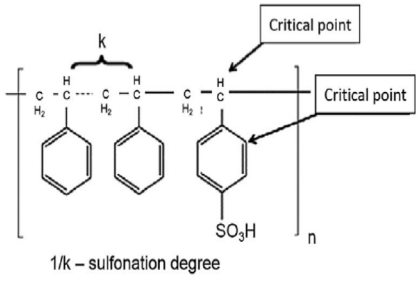


(e)

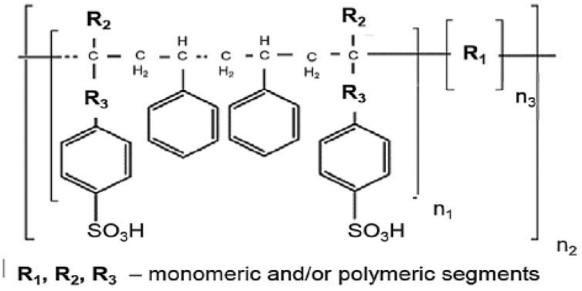


(f)

**Fig. 9.** Chemical structure of some typical alternative membranes for Nafion (Scofield et al., 2015): (a) Polybenzimidazole-based (PBI) membranes; (b) Polyphenylsulfone membrane; (c) SPEEK membrane; (d) Phosphonic-based membranes; (e) Polyphosphazene-based membranes (SPE); (f) Polystyrene sulfonic acid (PSSA) membranes.

stability, accounting for more than half of the catalyst production cost. Some attempts to lower cost and enhance the durability of electrodes were made by seeking solutions to overcome challenges stemming from PEMFC utilization. Many researchers are focusing on finding cheaper and durable substitutes for platinum, although they may not exhibit a comparable performance to that of platinum. These catalysts fall into three categories (Table 3): platinum-based catalysts; modified platinum-based catalysts containing other metals, such as Cr, Cu, or Co; and nonplatinum-based catalysts, such as non-noble metal or organometallic catalysts (Zhang et al., 2009).

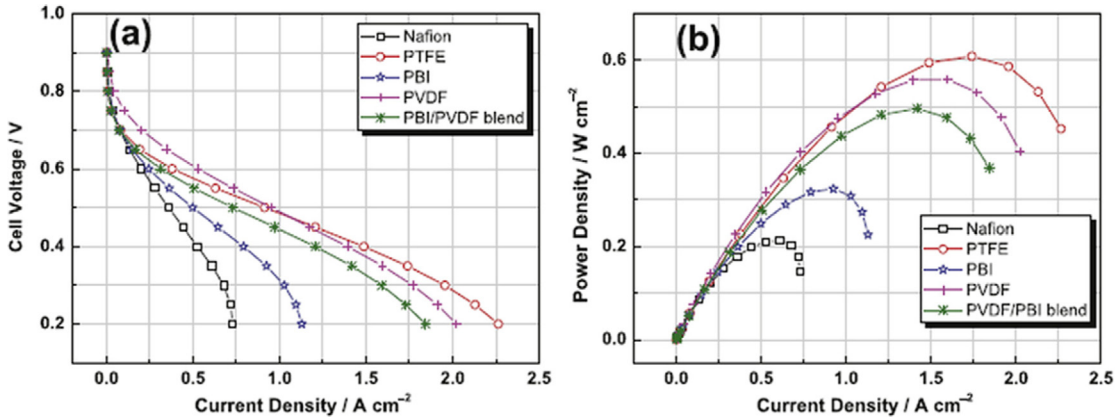


**Fig. 10.** Cell performance recorded under varying polymer binders at 160 °C (Su et al., 2013): (a) polarization curve and (b) power density.

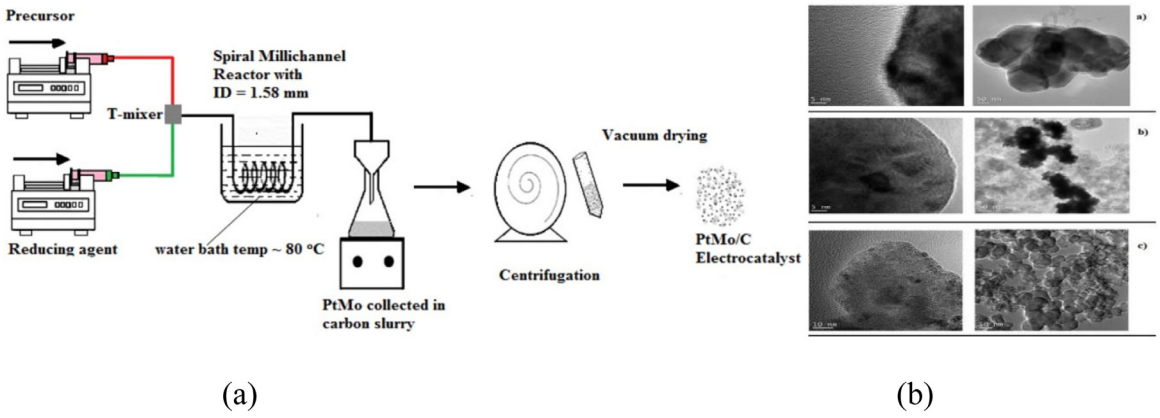


**Fig. 11.** Preparation and characterization of Pt-Mo/C catalysts: (a) Schematic diagram of an experimental setup with fabricated millichannel reactor for the synthesis of Pt-Mo/C catalysts; (b) Transmission electron microscopy (TEM) images of synthesized Pt-Mo/C catalysts at different metal loadings (Pillai et al., 2019).

**Table 3**
Categories of catalysts.

| Category | Platinum-based catalysts | Modified platinum-based catalysts | Non-platinum-based catalysts |
|---|---|---|---|
| Metal element | Pt | Pt, Cr, Cu, Co, Ru, Pd, Ni | Non-noble metal |
| Cost | High | Medium | Medium |
| Efficiency | High | Medium | Medium |
| Research status | Dominant | Under research | Under research |
| Durability | Relatively high | Needs to be proven | Needs to be proven |
| Weakness | High cost; poisoned easily; resource shortage | Low catalyst activity, the durability needs to be proven | Low catalyst activity; without application in practical area |
| Strength | High efficiency; good performance; widely used in practice and fully researched | Low cost; improved catalyst performance to increase the size of active catalyst site | Low cost; some specific catalyst has similar performance to Pt in experiment |

As the most effective catalysts, platinum-based catalysts have dominance in research, including typical studies on improving both morphology and synthetic protocols (Scofield et al., 2015). The type of carbon substrate, CL and catalyst properties, different surface structures, placement of CL, and other factors have been studied to explore their influences. Additionally, current studies are focused on developing modified carbon-based or non-carbon-based materials as catalyst supports to promote the catalytic performance of Pt (Samad et al., 2018). It has been proven that the utilization of platinum alloys has a positive effect on promoting the catalytic performance by increasing the active catalyst size, while its durability has yet to proven. Meenakshi found that the Pt3Sc/PECNT cathode catalyst exhibited a high oxygen reduction reaction (ORR) activity and higher power density (760 mW cm$^{-2}$ at 60 °C) in single-cell measurements (Garapati and Sundara, 2019). Fig. 11 depicts the fabrication method of nano-sized Pt-Mo/C catalysts, as well as the influence of Pt loading and distribution on performance, indicating that nanoparticles can reduce the utilization of noble metals and thereby reduce cost (Pillai et al., 2019).

Developing platinum group metal (PGM)-free and iron-free electrocatalysts is of great significance to break the barrier of high cost and short-term durability of PEMFCs imposed by PGM. High-temperature pyrolyzed FeN(x)/C catalysts have been recognized as effective nonprecious metal electrocatalysts for ORR, and have attracted considerable attention from researchers. Wang et al. (2014) explored an FeN(x)/C catalyst derived from poly-m-phenylenediamine (PmPDA-FeN(x)/C) with higher ORR activity

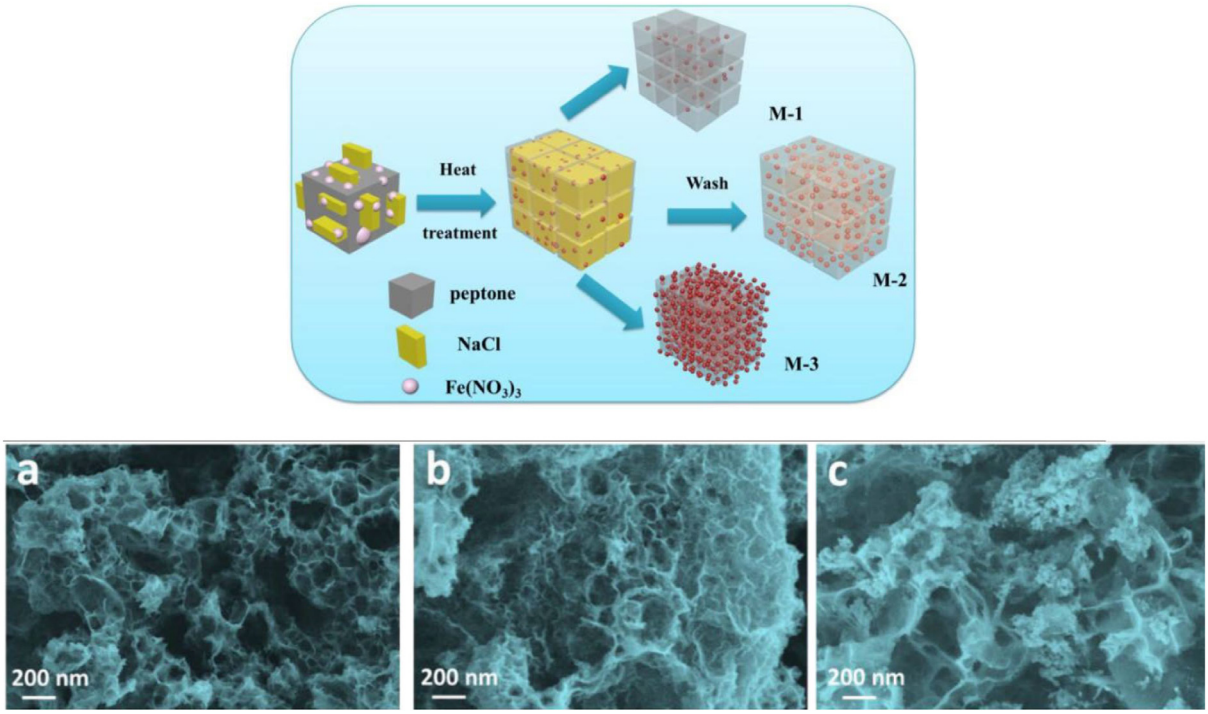


**Fig. 12.** Schematic of fabrication procedure of (FeNx/C) and SEM images (Ding et al., 2019).

(11.5 A $g^{-1}$ at 0.8 V vs RHE) and a lower $H_2O_2$ production rate (<1%). Liu et al. (2019) conducted computational and experimental research to study the activity, mechanism, and durability of Mn and N co-doped carbon (denoted as Mn–N–C), and the results suggest that Mn–N–C would exhibit a high catalytic performance for ORR in an acidic medium. A high-temperature approach was employed to synthesize an Mn–N–C catalyst via a polymer (i.e., polyaniline-PANI) hydrogel precursor, indicating the possibility of atomically dispersed Mn sites coordinated with N being formed in the catalyst and the superior potential cyclic stability of the Mn–N–C catalyst. However, it is still a challenging task to use nonplatinum catalysts, as their durability and performance remains to be investigated. N-doped iron-based carbon materials (FeNx/C) can be fabricated by employing peptone as a precursor and molten salt, NaCl, as a template, providing a more environmental friendly and low-cost method of catalyst preparation. It can be seen in Fig. 12 that there are more nanoparticles in M-2 in comparison with the others (Ding et al., 2019).

At present, nonplatinum-based catalysts and modified platinum-based catalysts are promising substitutes; however, there is still a long way to go before they may be employed in practical manufacturing and industrial applications. Different materials have been tested for whether they can be applied in fuel cells with good work efficiency, and a breakthrough will be required to solve the catalyst issue of finding a substitute for platinum. For example, sludge biochar-based catalysts (SBCs) can be employed as an electrode material in a microbial fuel cell (MFC), and this scale of rich carbon and metal content in SBCs is more suitable to serve as a catalyst, owing to both the adsorptive and catalytic properties (Huang et al., 2017).

### 2.4. Gas diffusion layer

GDL is responsible for underpinning the homogeneous distribution of the reaction gas on the catalyst surface, as well as removing water from the catalyst surface. Generally, as shown in Fig. 1, the GDL is a hydrophobic channel that has been treated with hydrophobic water and connects bipolar plates with the CL. PTFE is a commonly used water repellent, and a hydrophilic channel that is not treated with hydrophobic water acts as a water transfer channel. Drainage, gas permeability, and electrical conductivity are three compulsory conditions for GDL. Thickness is an important factor that has a significant effect on the above three elements, because if the GDL is too thick, the mass transfer resistance increases and the mass transfer progress is delayed; if the GDL is too thin, there is an increased probability of leakage of the catalysts and the tri-phase reaction area decreases. The thickness of the GDL is the sum of the thicknesses of the microlayer and macrolayer; Mosdale and Srinivasan (1995) proposed the following semi-empirical equations:

$$E = E^0 - b\log i - Ri \tag{1}$$

$$E = E^r + b\log i^0 \tag{2}$$

where $i$ is the current density and $E$ is the cell potential. $E^r$ is the reversible potential for the cell, $b$ and $i^0$ are the Tafel parameters for ORR, and $R$ stands for the Ohmic resistance.

To evaluate the dynamic flow in the GDL, the formulae (Sitanggang et al., 2009) shown below are used to express the gas concentration in the GDL (C) and the effective gas distribution ($D_{eff}$) through the GDL pores.

$$C = \varepsilon C_f + (1-\varepsilon)\rho_s C_s \tag{3}$$

$$D_{eff}\frac{d^2C_f}{dt^2} - \nu\frac{dC}{dt} = 0 \tag{4}$$

Here, $\varepsilon$ is the porosity, $C_f$ represents the gas concentration in the fluid within the GDL void, $Cs$ is the gas concentration in the GDL–solid interface, $\rho_s$ is the mass density of the solid phase, $v$ is the flow velocity, and $t$ is the time.

There are four types of GDL configurations, as shown in Fig. 13(a), namely, two layers of (CC), a layer of the mixture of carbon–polymer and carbon cloth (CPCC), two layers of carbon–polymer (CP) and CPCC, and four layers in the order of CP-CPCC-CC-CPCC; an X–Y robotic spraying technique can be used to

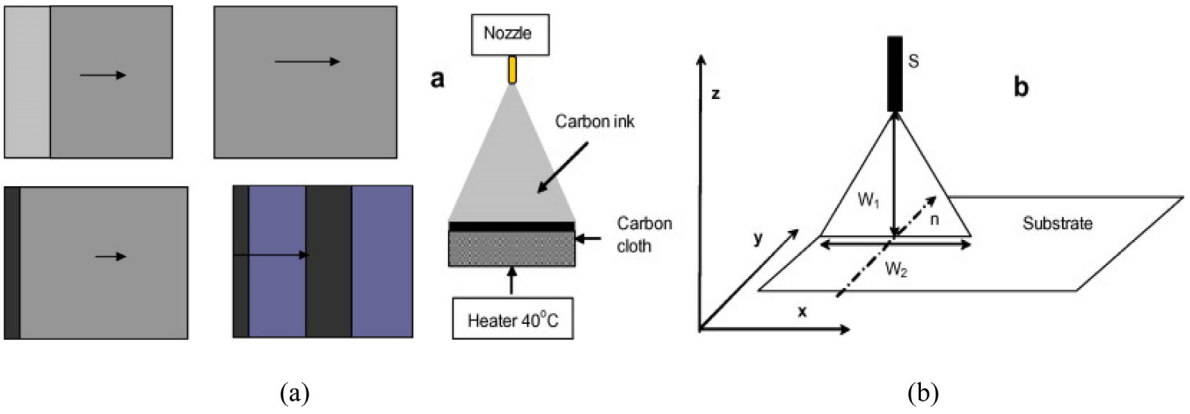


**Fig. 13.** Four types of GDL structural configuration (a) and the schematic of spraying fabrication method of GDLs (b) (Sitanggang et al., 2009).

**Table 4**
Comparison of the GDL produced by Toray (Japan) and SGL (Germany).

| Parameter | Unit | Toray (TGP-H-030) | SGL (22B8) |
|---|---|---|---|
| Thickness | mm | 0.11 | 0.215 |
| Density | g $cm^{-3}$ | 55 | 70 |
| Tensile intensity | MPa | 0.4 | 6.9/4.6 |
| Electronic resistance | Ω cm | 80 | 33 |
| Porosity | % | 80 | 78 |
| Thermal conductivity (room temp.) | W $(m\ K)^{-1}$ | 21 | 0.3 |

**Table 5**
DOE targets of BPs for transportation applications.

| Parameter | Units | 2015 status | 2020 target |
|---|---|---|---|
| Cost | \$ $kW^{-1}$ | 7 | 3 |
| Plate weight | kg $kW^{-1}$ | <0.4 | 0.4 |
| Plate $H_2$ permeation coefficient | Std $cm^3$ ($s^{-1}$ $cm^{-2}$ Pa)@80 °C, 3 atm 100RH | 0 | $<1.3\times10^{-14}$ |
| Corrosion, anode | $\mu$A $cm^{-2}$ | No active peak | <1 or no active peak |
| Corrosion, cathode | $\mu$A $cm^{-2}$ | <0.1 | <1 |
| Electrical conductivity | S $cm^{-1}$ | >100 | >100 |
| Areal specific resistance | Ω $cm^{-2}$ | 0.006 | <0.01 |
| Flexural strength | MPa | >34 (carbon plate) | >25 |
| Forming elongation | % | 20–40 | 40 |

fabricate a GDL by spraying carbon ink on a heated CC and then drying (Fig. 13(a)) (Sitanggang et al., 2009). The carbon powder can influence the pore structure of the prepared GDL significantly owing to the difference in physical properties, such as the specific surface area, pore distribution, particle size, and electrical conductivity. At present, Vulcan XC-72R (specific surface area 250 $m^2$ $g^{-1}$, particle size 30 nm) and Acetylene Black (specific surface area 50–70 $m^2$ $g^{-1}$, particle size 40–50 nm) are commonly utilized in PEMFCs. In Ballard mark V cells, carbon cloth provides an outstanding advantage at high current densities, and has been shown to be more efficient for the transport of liquid water owing to the hydrophobicity of the cloth surface. Lin and Chang (2015) examined an MPL composed of a composite carbon material with multiwall carbon nanotubes (CNTs) and acetylene black (AB) and compared the results with the cases of MPLs made with pure AB and CNT. Their experiments demonstrated that the cathode MPL with a mixing ratio of 1:4 of AB and CNT by mass demonstrates the best performance in all cases. Toray (Japan), SGL (Germany), Zenyatta (Canada), Ballard (Canada), and Freudenberg (Germany) are the companies that produce GDLs, and the properties of two GDLs are presented in Table 4.

### 2.5. Bipolar plate

Bipolar plates (BPs) of PEMFCs have the following functions and features.

a. Connecting a series of single cells to form a stack and collecting and transporting the generated current from one cell to the next cell. Therefore, durability and electrical and thermal conductivity are the required characteristics of BPs.
b. Evenly distributing fuel gas on the anode surface and oxygen on the cathode surface. This prevents the formation of a hot spot, whereby a faster chemical reaction rate exists, generating a higher current density and damaging the cell.
c. Distributing reactant gas through electrodes where electrochemical reaction occurs and removing unused gas and water. Liquid water can be produced because PEMFCs normally operate below 100 °C and should be removed effectively to avoid water flooding in the CL and GDL.
d. BPs are exposed to water and gas phases under relatively high temperature and humidity, and thus good thermal conductivity and mechanical strength to remove heat and support the stack are required to ensure a long lifespan.

**Table 6**
Properties of three typical bipolar plates.

| Category | Non-porous graphite plates | Surface-modified metal plates | Composite bipolar plates |
|---|---|---|---|
| Material | Toner or graphite powder and graphitizable resin | Al, brass, Aluminum alloy, Ti, 316# stainless steel | Metal plates and graphite plates |
| Thickness | about 3 mm | 3–5 mm | 1–2 mm |
| Character | Small resistance, light weight, corrosion resistant but high cost, weak intensity | Easy preparation process, high intensity, small size but heavy weight, corrosive | Corrosion resistant, small size, light weight and high strength |
| Processing methods | Machining, injection molding | Machining, stamping | Injection molding, roasting |

Evenly distributing fuel gases, maximizing the reaction area, minimizing the total resistance, transporting the proper amount of water, and simple manufacturing in large scales have made it a long and difficult path to optimize the flow field design in BPs. The requirements for BPs as summarized by the Department of Energy (DOE) are presented in Table 5, which indicates that the focus of BP design is switching from reducing resistance to enhancing water removal, and now to enhancing mass transfer.

The most widely used material is graphite with its properties of hydrophobicity (85° contact angle), noncorrosivity, and easy manufacturability, whereas metals of higher conductivity, such as aluminum, are applied in BP production and must be coated with anticorrosion paint to prevent corrosion. BP materials widely used in PEMFCs include nonporous graphite plates, surface-modified metal plates, and composite BPs, whose properties are summarized in Table 6. A (2001) proposed a 0.25 mm graphite plate composed of graphite flakes or graphite powder as a support layer with a total BP thickness of 1.0 mm, the flow channel pressed with carbon cloth, and the frame made of polycarbonate. The sealing is realized by silicone rubber, and the heat removal is achieved using a heat extraction film. This design significantly increases the volumetric specific power of the cell with a fiber reinforcement structure (Chini and Fabrizio, 2019) containing thermoplastically bonded carbon fibers. The fiber reinforcement structure is multilayered and comprises a plurality of fiber reinforcement layers, including two or more thermoplastically bonded carbon fibers. Composite plates can increase the volumetric power and mass ratio power of a cell, and combine the advantages of graphite and metal plates by using a thin metal plate or other high-strength conductive plate as a partition plate and a graphite plate as a flow field plate. MERCURI et al. (2000) prepared a composite plate as follows: First, ceramic fiber (1.5%–5% mass percentage) with a length of 0.15–1.5 mm and a width of 0.04–0.004 mm, natural graphite, and resin (15% mass percentage) are mixed and dried at 100 °C. Then, they are pressed into a flow field of a certain shape and heated to 1115.74 °C to expand the volume of the graphite scale to 80–1000 times the original volume. The ceramic fiber is surrounded by a flow field plate with a total thickness of 1–1.5 mm. Because the support portion of the flow field plate is very thin (0.05–0.2 mm), the intensity is low. A dense, high-strength, thin graphite plate is prepared as a support plate for the flow channel plate, with a thickness of 07–0.15 mm.

In general, nonporous graphite plates can adjust the electrical conductivity and mechanical intensity of the BP according to the ratio of the conductive filler and the resin, and can also be mass-produced by using molding or injection-molding processes, thereby reducing the manufacturing cost of the BP. Selecting suitable conductive fillers and resins, improving the uniform mixing of carbon materials and resins, and optimizing the preparation process, enables the realization of composite BPs with high electrical conductivity and mechanical strength. The structure and preparation process of surface-modified metal plates are complicated by high manufacturing cost and it is difficult to conduct mass production. Composite BPs combine the advantages of graphite BPs and metal BPs, and are suitable for applications in which high corrosion resistance, high electrical conductivity, and high intensity are required. Additionally, appropriate coatings have the potential to prevent corrosion and improve performance.

### 2.6. Flow channel

Flow channels are utilized for removing water, and delivering and distributing reactants to the MEA, whereas the region between the flow channels is used for collecting and transporting current from one cell to another and transferring the heat generated in the MEA. The flow channel is the only part that exchanges mass and removes moisture from the system. If the moisture in the flow channel cannot be removed in time, it will not only affect the transmission of the reaction gas, but also increase the system pressure drop, make the current distribution uneven, lower the performance, and, even more critically, adversely affect the operation safety. Kahraman and Orhan (2017) experimentally studied three main flow field channels and indicated that water would accumulate and cause flooding in the center of a parallel flow field, downstream channels of an interdigitated flow field, and corners of serpentine flow field channels. The structure of a flow channel determines the flow state of the reactants and products in the flow fields. Table 7 presents a comparison of several typical types of flow field plates. A well-designed flow field plate should be able to: (1) evenly distribute the fuel and oxidant required for fuel cell discharge to ensure uniform current density distribution and avoid local overheating, (2) make the fuel cell generate water smoothly under the reaction exhaust purge and entrainment exclusion, which requires the fluid to have a certain linear velocity in the flow channel.

### 2.7. Thermal management

Thermal management concerns the generation and transmission of heat in the cell, the temperature field distribution, and the cooling method. According to the cooling medium, the cooling method of a fuel cell is categorized into three types: liquid coolant cooling, phase change cooling, and air cooling, as shown in Fig. 14. Air cooling methods include cathode air cooling, reactive air, and cooling air separation, which are suitable for small fuel cell systems of less than 100 W and 100–1000 W, respectively. In comparison with air cooling reactors, water cooling reactors are widely used in practical appliances, owing to their smaller size, more compact structure, and higher specific heat capacity. The main source of heat is from Ohmic heat and reaction heat, which is similar to the power from $H_2$ and $O_2$ subtracting the output power, and it can be calculated as follows:

$$Q_g = (1.2 - V_{cell})\, In_{cell} \tag{5}$$

where $Q_g$ is the power of residual heat, $V_{cell}$ is the transient output voltage for the fuel cell system, and $In_{cell}$ is the transient output current for the fuel cell.

**Table 7**
Comparison of several typical types of flow field plate.

| # | Design | Schema | Description | Advantages | Disadvantages |
|---|---|---|---|---|---|
| 1 | Porous material (MERCURI et al., 2000) | 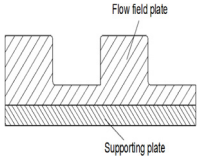  | Parallel or serpentine plates with landings containing many small hydrophilic capillary columns | Good performance with high current densities and good water removal | High cost and hard to produce |
| 2 | Pin type (Reiser and Sawyer, 1988) | 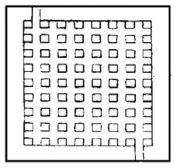 | Grooves formed by the grids protruding from the channels | Low pressure drop, fit for high reactants | Uneven distribution of current density, reactants and water removal |
| 3 | Mesh type (Mahlou, 1998) | 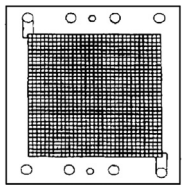 | Porous metal mesh structure | Good performance under limited current densities, low pressure drop and controllable contact area | Corrosion issues, poor water removal and difficult to manufacture |
| 4 | Parallel (Voss and Chow, 1993) | 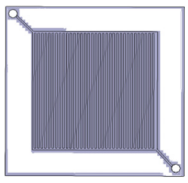 | Parallel channel | Low pressure drop and homogeneous gas distribution | Inhomogeneous water removal, water blockage and Low channel velocity |
| 5 | Criss-cross (W, 1996) | 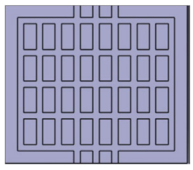 | Modified channel where the gas and moisture are mixed | Similar advantages to parallel and improved water removal | Similar disadvantages to parallel |
| 6 | Single serpentine (Wilkinson et al., 1996) | 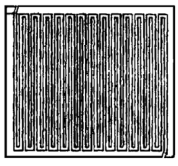 | A constant path during the whole progress | Good water removal for high channel velocity and widely used in small active areas | Uneven distribution of reactants, high pressure drops and air oxidant issues |
| 7 | Parallel serpentine (Kirk, 1994) | 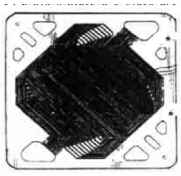 | Several continuous paths from start to end | Less pressure drop than single serpentine, optimum for large active areas and adequate water removal | Relative high pressures because of path length and uneven distribution of reactant |
| 8 | Mirror serpentine (William, 1999) |  | Modified serpentine where the near serpentines are mirror images of each other | Less pressure drop than single serpentine, optimum for large active areas with multiple inlets and outlets | Combination of disadvantages of single and parallel serpentine |

(*continued on next page*)

**Table 7** (*continued*).

| # | Design | Schema | Description | Advantages | Disadvantages |
|---|---|---|---|---|---|
| 9 | Radial (Yoshiake, 1999) |  | Standard circle with a set of radial flow rings | Improved mass transport, water removal, current density, performance and reasonable pressure drop | Just under development and experimentation and membrane drying-out |
| 10 | 3D flow field (Shen et al., 2020) | 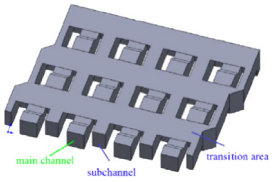  | Several straight flow units in a staggered manner with an inclination at the end | Effectively separate liquid water from the reactant flow; enhance the mass transfer ability and improve the PEMFC performance, especially at high current densities | Too complex structure to be fabricated for large-scale commercialization |

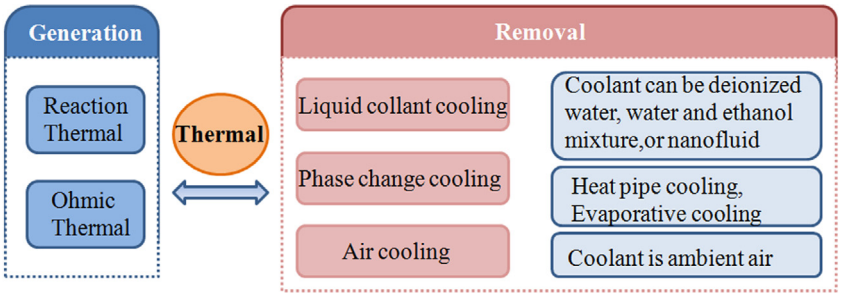


**Fig. 14.** Scheme of thermal production and removal.

There are three main ways in which the residual heat of the fuel cell can be discharged from the stack: internal water vaporization $\Delta Q_w$, heat radiation $\Delta Q_r$, and external circulating cooling water to take away heat $\Delta Q_c$. The heat balance can be calculated as follows:

$$\Delta Q_w = \lambda k(m_{O_2} + m_{H_2})/3600 \tag{6}$$

$$\Delta Q_r = \delta\sigma A_r(T_{cell}^4 - T_0^4) \tag{7}$$

$$\Delta Q_c = \mathrm{cnA_c}\nu\rho(T_{out} - T_{in}) \tag{8}$$

$$\sum \Delta Q_i = Q_g \tag{9}$$

where $\lambda$ is the thermal conductivity, $m_{O_2}$ and $m_{H_2}$ are the overall masses of $O_2$ and $H_2$, respectively, and $\delta$ is the radiation blackness for the fuel cell system. $\sigma$ is the Stefan–Boltzmann constant, $5.67\times10^{-8}$ W m$^{-2}$ K, $c$ is the specific heat capacity of the coolant, n is the number of flow channels, $A_c$ is the area of each channel, and $A_r$ is the total area of radiation.

Mahjoubi et al. (2019) investigated the thermal management of an open cathode PEMFC. Based on system thermal balance and operating constrains, an optimal operating zone controlled by loading current, stack temperature and air stoichiometry, has been designed. Temperature gradient is the direct expression of thermal management. Wang et al. (2019c) proposed a water and thermal comfort index, which will increase at first and decrease after keeping steady for a while with raise of temperature, to reflect the water and thermal condition in PEMFC. The comfort index(R) in their work is expressed as,

$$R{=}R_{Lqc}{+}R_{\gamma acl} \tag{10}$$

$$R_i{=}A_iU_i(i{=}L_{qc}\mathrm{or}\gamma_{acl}) \tag{11}$$

where $U_i$ represents the degree of comfort index and water flooding and anode drying, $A_i$ is the weight coefficient, and $L_{qc}$ is the minimum amount of removed liquid water needed to ensure that no flooding occurs in the cathode channel, which is the sum of water vapor condensation and GDL to the channel. Generally, the condition can be regarded as comfortable when the index value is higher than 0.8. The temperature gradient of the membrane electrode of the fuel cell under non-humidified conditions was measured by Wang et al. (2008) using infrared imaging technology. The experimental results demonstrated that the downstream temperature of the fuel cell is higher than the upstream temperature, and as the current density increases, the temperature of the membrane electrode increases, and the uniformity of the temperature distribution deteriorates. By establishing a mathematical model, one can obtain a clearer understanding of the internal chemical reaction procedure in a cell, learn about the influence of different parameters on fuel performance, and provide useful guidance to the structure design and performance optimization. Zhang and Jiao (2018) suggested that, to investigate the influence of thermal management in PEMFC more accurately, a three-dimensional (3D) multiphase computational fluid dynamics (CFD) simulation should be conducted at the cell level and stack level with the consideration of coolant channel and heat convection thermal boundary conditions. Zhao et al. (2015) proposed a thermal management model, which was verified by an experimental system, including a coolant circulation pump and radiator fan, under three different operation conditions, to help design and optimize a water-cooled PEMFC control system. Strahl and Costa-Castelló (2016) studied a system model, consisting of two dynamic parameters of the fuel cell temperature and the liquid water saturation, to improve the thermal management of an open-cathode PEMFC. The results demonstrated that the maximum power is achieved in a moderate temperature region and the phase plane is decomposed into stable and unstable parts by maximum power line decomposition.

The balance between heat generation and removal determined the operating temperature and thermal distribution. At present,

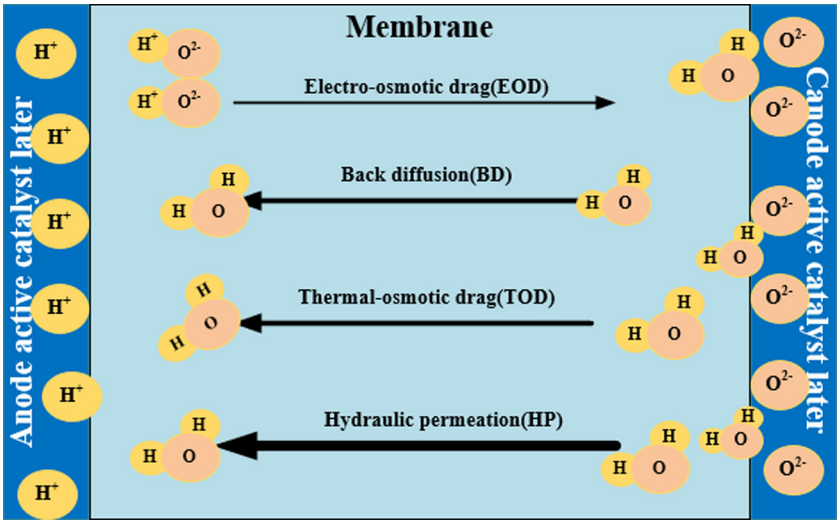


**Fig. 15.** Water movements in PEMFCs including EOD, BD, TOD, and HP.

water cooling is the main tool for thermal removal. Electrolyte dehydration and cathode flooding caused by the nonuniform temperature distribution which exists in the vertical (across the membrane) and horizontal (along the flow length) directions become the most critical challenges for PEMFCs.

### 2.8. Water management

As the main product of operation in a fuel cell system, water exists in all parts of its key components. Therefore, it is of great importance to manage water transport well to maintain efficient and stable operation of PEMFCs. Studying the liquid water transport characteristics in the flow channel and optimizing the water management have a guiding significance for the design of PEMFCs (Hassan et al., 2009). Water is transported in a PEMFC by many different mechanisms, such as electro-osmotic drag (EOD), thermal-osmotic drag (TOD), hydraulic permeation (HP), and back diffusion (BD) (Ijaodola et al., 2019). Fig. 15 shows the mechanisms by which water can be transported in PEMFCs. TOD appears because of the temperature difference in a membrane, where water flows from a cold area to a hot area. Richard et al. indicated that the effect of a heat pipe also occurs in the CL of a PEMFC, which becomes one of the most important factors of TOD. A mode of great importance during start-up and shut-down was constructed to describe the evaporation of water that moves as vapor then condenses down a path as a result of a temperature decrease given by the temperature gradient in the cell. The process of water transport across the membrane due to dragging by protons is called EOD, which is relevant to the relationship between proton conductivity and humidity. The EOD coefficient is defined as the moles of water transferred across the membrane by 1 mole of protons. Park and Caton (2008) conducted an experimental study on EOD coefficients of Nafion 115 obtained under several different operating conditions. Their results showed that EOD varied from 0.82 to 0.50 and the current density varied from 0.4 to 1.0 A $cm^{-2}$, indicating that EOD has a negative correlation with current density. Water is generated at the cathode in excess of that at the anode and this force is called BD (Zhao et al., 2011). A pressure gradient exists between the anode and cathode, resulting from a capillary pressure difference or gas phase pressure difference. As a result, HP occurs and can be measured by the methods of liquid–liquid and liquid–vapor permeation (Wakita et al., 2019).

The water movements are difficult to observe and predict during operation, owing to the two-phase flow. Methods of in-situ visualization of liquid water have been reported, which include nuclear magnetic resonance imaging (Shim et al., 2009) and beam interrogation (Tüber et al., 2003) techniques, such as X-ray (Sasabe et al., 2010), neutron imaging (Boillat et al., 2008), and high-speed photography (Afra et al., 2019). Apart from for tools, specially made transparent single cells (Lee and Bae, 2012) have been made to visualize the water flooding, although it is difficult with a transparent cell to observe water movements accurately. A transparent PEMFC was designed, manufactured, assembled and tested to study its water management and contact resistance in a dead-end mode (Rahimi-Esbo et al., 2017).

To understand the water flow in PEMFCs, Nikiforow et al. (2014) set a water content distribution model along the flow channel in the cathode and anode with flow fully developing at a steady state. They concluded that using dry air and saturating the hydrogen feed would prevent flooding and the formation of a water droplet. EOD and BD are recognized as the dominant mechanisms for water transport within the membrane. To analyze the mechanism of water transport, Wu et al. (2009) proposed an unsteady nonisothermal 3D model demonstrating that the cell current output response time is influenced by the finite rates of sorption/desorption of water, and the relative permeability exhibited greater effects on the liquid water transport than the capillary pressure. Srinivasan et al. (1989) analyzed the water transport flux in different water activity membranes in a constant state experimentally and theoretically, and obtained the relevant adsorption, desorption, and diffusion coefficients. The results show that the desorption coefficient of water differed from the adsorption coefficient by an order of magnitude; that is, the water loss rate of the saturated humidified membrane is much larger than the membrane adsorption moisture velocity, illustrating the imbalance of water absorption and water loss of the membrane.

The water production from the electrochemical reactions leads to nearly unavoidable water condensation; liquid water may be present and flood the electrode pore regions, so-called water flooding, which severely reduce the rate of reactant supply to the reaction sites and degrades the cell performance considerably. Poor mass transport and carbon corrosion also occur in the stack because of water flooding. According to the principle of bionics, a three-step water removal was realized by Chen et al. using the gravity of the droplet itself to overcome the viscous force and realize the self-removal of the droplet (Chen et al., 2015).

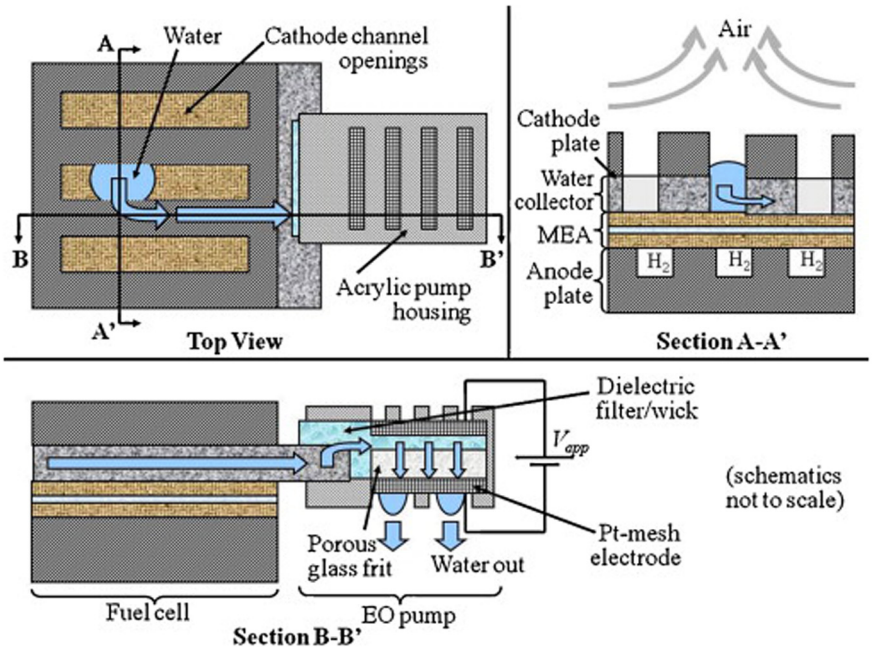


**Fig. 16.** Schematic diagram of PEMFC flow channel with water collector and electroosmotic pump structure (Fabian et al., 2006).

A new type of BP proposed by Fabian can promote the water removal ability (Fig. 16). The structure mainly includes a layer of conductive hydrophilic wick laid on the bottom of the flow channel and an electroosmotic pump. When liquid water appears on the membrane electrode, it is be absorbed by the hydrophilic water collector and discharged along the wick structure under the action of the electroosmotic pump (Fabian et al., 2006).

Maintaining sufficient moisture in the PEM is a prerequisite for proper FC operation. In the past, internal and external humidification approaches were usually employed to maintain the humidity of the membrane, because the immature fuel cell technology caused low current density and the amount of water generated was insufficient to maintain the normal operation of the membrane. In modern systems, the water generated inside the stack is sufficient to wet the membrane electrode with the substantial increase in the power density of fuel cell stacks. In the future, Toyota will use a hydrogen circulation pump to humidify the PEM with a humidified hydrogen cycle, thereby eliminating the humidifier and greatly reducing the complexity of the stack, whose principle is the same as that of the self-humidification method. It is clear that self-humidification technology will become the mainstream direction of humidification methods in the future. The principle of water management is to maintain the balance of water generation and removal, and the material and assembly must satisfy the needs of the load and working conditions. However, the research on water transport mechanisms is insufficient to establish a complete water transport model, and thus more work is still required in this area.

### 2.9. Fuel cell vehicle

FCV is of great important in many countries to release the environment stress and decrease the consumption of fossil fuel (Tanç et al., 2019). Some representative automobiles are shown in Fig. 17. There are more than 60 fuel cell buses in Europe, especially in London, where the fuel bus has been placed in service for more than 15 years under the CUTE program. The similar step has been taken by China. With the support of Chinese new energy vehicle program, about 30 fuel cell buses has been in service in 2017 and the largest fuel bus project around world has been executed in Foshan, with a 5000 fuel cell buses production ability per year (Kendall, 2018).

Generally, FCV refers to a vehicle using a fuel cell as part of the power system, and can be classified as pure FCV (PFCV) and fuel cell hybrid electric vehicle (FCHEV). FCHEV is the vehicle combining the fuel cell and other energy storage system, which can be categorized as fuel cell + flywheel (FC+FW), fuel cell + battery (FC+B), fuel cell + ultracapacitor (FC+UC) and fuel cell + battery + ultracapacitor (FC+B+UC) vehicles (Das et al., 2017). In fact, fuel cells, particularly PEMFCs, are used as a major source to supply the systems, and Li batteries and ultracapacitors are installed as a backup system to deal with the peak power and fast transient condition in FCHEVs (Gherairi, 2019). Table 8 shows the running range in one time fueling and fuel economy under city and highway usage of some commercial FCVs since 2014, using hydrogen as fuel. From Table 8, the maximum running range is up to 435 miles in a single refueling, and Toyota Mirai achieves the best fuel economy with 66 MPGe under both city and highway usage. The operating mode of Mirai and Honda was chosen as PFCV for their PEMFCs have better dynamic characteristics, while these of Audi A7h and Honda clarity choose PCHEV mode for better acceleration to make up the instability during operation. To overcome the disadvantages of FCHEVs, some of the most common control strategies are introduced simultaneously: peaking power source strategy, operating mode control strategy, fuzzy logic control strategy, and equivalent consumption minimization strategy (Manoharan et al., 2019). By programming the detailed model of FCHEVs in MATLAB/Simulink, Arruda et al. (2016) found that FC+B and FC+B+UC vehicles were equally suitable for practical application, because FC+B vehicles are normally less expensive, whereas FC+B+UC vehicles have lower operation cost owing to higher fuel efficiency and longer fuel cell lifetime. In order to optimize an FCHEV system, Wang et al. (2019b) proposed a semi-theoretical and semi-empirical model considering the cell degradation and deterioration of the fuel cell to extend its lifespan.

As the latest technical targets of DOE, the developing requirements for light-duty vehicle (Fig. 18) and Long-Haul Tractor-Trailers (Table 9) are changing as well; however, longer lifetime, lower system cost, and higher system efficiency remain the perennial goals in the fuel cell field, regardless of the type of FCV.


**Fig. 17.** Representative FCVs: Toyota Mirai, Honda FCV Concept, Roewe 950, and Audi A7 (The specific power density of Roewe 950 and Audi A7h are not given in public resources) (Nonobe, 2017).

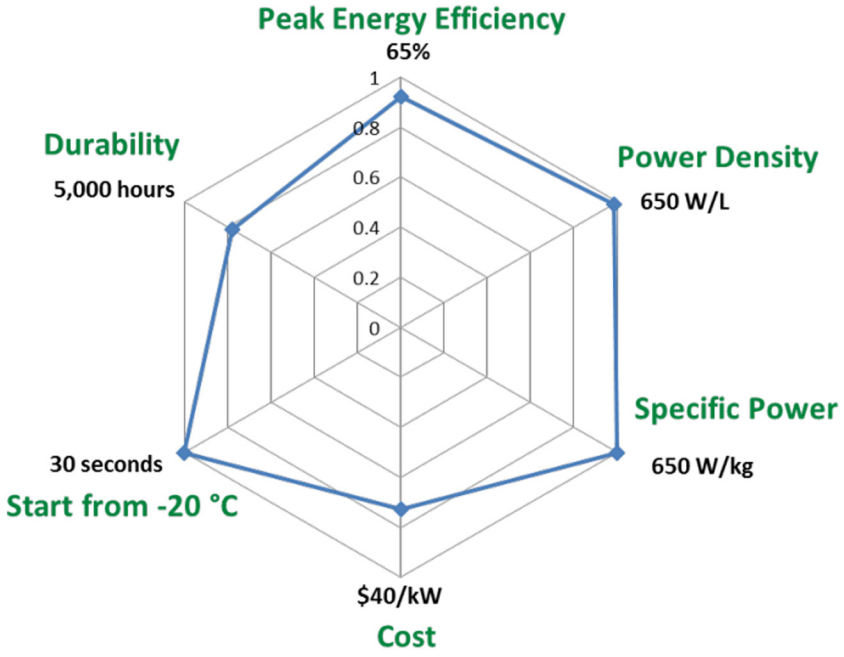


**Fig. 18.** Fuel cell power system target versus 2015 status (blue) for light duty vehicle applications according to DOE (cost is based on a manufacture volume of 500,000 units per year). (Blue lines are the 2015 status, and numbers at the hexagon vertices are the targets.)

Some studies have been carried out to evaluate the market possibility of FCVs in different countries. Kim et al. evaluated the preferences of South Korean people regarding FCVs by using a choice experiment. Interestingly, the results showed that a decrease of air pollutants had higher weight than other factors and SUV FCVs were more popular than sedan FCVs (Kim et al., 2019). Moreover, Brey et al. (2018) investigated the marketability of FCVs in Spain through a case study considering both investors and consumers. In the case study, they found that an initial investment of 24–25 million euros would be sufficient to build up the infrastructure and hydrogen would be as competitive as gasoline for the consumer with the appropriate government policy.

To commercialize the FCV, one of the important supporting facilities is the hydrogen station to refuel the vehicle. The state of California is the representative region, which has built up 51 hydrogen stations, consuming nearly 63,000 kg hydrogen by 2014, and another 46 hydrogen stations have been planned (Sprik et al., 2015). In addition, the US government plans to establish an energy network in California by building approximately 10,000 hydrogen stations by 2050 (Anon, 2016a). Similarly, Japan has claimed that 100 hydrogen stations will be established by 2015 (Holloway, 2015) and other 80 hydrogen stations are planned by the Japan Hydrogen Mobility consortium by 2021 (Anon, 2018c). In Germany, Linde AG of Germany and Air Liquid of France collaborated to achieve significant progress by

**Table 8**
Summary of commercial FCVs.

| Vehicle prototype | Year | Running range (mile) | Fuel economy MPGe at city | Fuel economy MPGe at highway | Type |
|---|---|---|---|---|---|
| Honda FCX clarity (Energy, 2016; Anon, 2015c) | 2014 | 231 | 58 | 60 | PFCV |
| Honda FCV Concept (Anon, 2015c) | 2014 | 435 | / | / | PFCV |
| Audi Sportback A7h-tron Quattro (Anon, 2016b; VorsprungdurchTechnik, 2015; Anon, 2015b) | 2014 | 500 | 62 | 62 | FCHEV |
| Roewe 950 Fuel cell (Wikipedia, 2015) | 2014 | 350 | / | / | PRFV |
| Volkswagen Golf Hymotion (Anon, 2014c,a) | 2014 | 426 | / | / | PFCV |
| Toyota Mirai (Nonobe, 2017; Anon, 2016d) | 2020 | 750 | 66 | 66 | PFCV |
| Hyundai Tucson Fuel Cell (America, 2015) | 2016 | 265 | 49 | 51 | PFCV |
| Honda Clarity Fuel Cell (Anon, 2014b) | 2017 | 434 | / | / | FCHEV |

**Table 9**
Technical system targets: Class 8 Long-Haul Tractor-Trailers (updated 10/31/19).

| Parameter | Units | Targets for Class 8 Long-Haul Tractor-Trailers | |
|---|---|---|---|
| | | Interim(2030) | Ultimate |
| Fuel cell system lifetime | Hours | 25,000 | 30,000 |
| Fuel cell system cost | $ $kW^{-1}$ | 80 | 60 |
| Fuel cell efficiency | % | 68 | 72 |
| Hydrogen fill rate | kg $H_2$ $min^{-1}$ | 8 | 10 |
| Storage system cycle life | cycles | 5,000 | 5,000 |
| Pressurized storage system cycle life | cycles | 11,000 | 11,000 |
| Hydrogen storage system cost | $ $kW^{-1}$ ($ kg$^{-1}$ $H_2$ stored) | 9 (300) | 8 (266) |

increasing the number of hydrogen stations to 100 by 2017 and plan to achieve 400 stations by 2023 (Schwelm, 2009). The Korean government projects the construction of 100 hydrogen stations by 2020 (Yang et al., 2017). Though the FCV presents a fast-growing trend around the world, there are still many breakthroughs required to make it competitive with conventional automobiles. For example, hydrogen must be made as easily accessible as gasoline by establishing a hydrogen station network, fuel cells should have a long lifetime, and the energy management system is required to evaluate its high efficiency under real-time applications (Sulaiman et al., 2015).

The FCV is the key aspect of fuel cell commercial applications and a comprehensive system should be completed to make it practical for manufacturing. Durability, safety, hydrogen storage and refueling, system integration, and cost still are the focus areas of global FCV developers. Fortunately, the FCV attracts the attention of many national governments and much investment has been directed into this field. The research trend is toward efficient power conversion and effective controller design for the system and certain issues should be solved, such as hydrogen and oxygen regeneration, improving the transient performance of the system, and maximizing the fuel utilization.

## 3. Hydrogen technologies

Hydrogen is an ideal, highly efficient, renewable, clean, and sustainable energy carrier produced by electrolysis of water and thermochemical water splitting. Hydrogen possesses a high energy yield of 122 kJ $g^{-1}$, which is 2.75 times higher than that of hydrocarbon fuels (Demirbas, 2005). Hydrogen is recognized as an unsafe energy source for its higher flame temperature and explosion energy, wider ignition limits, and high diffusion coefficient. However, hydrogen-driven vehicles are found to be less dangerous than petrol vehicles, because the latter typically leak highly hazardous flammable gas, whereas the former cannot damage anything with their minor heat radiation, unless it is placed in flame immediately upon leakage (Lattin and Utgikar, 2006).

Technologies utilized during the progress of hydrogen generation, hydrogen storage, hydrogen transportation, and hydrogen application are collectively referred as hydrogen technology, which is a complex of multiple techniques. Hydrogen technologies are under active research in many countries, such as the US, Germany, China, Japan, Korea, and Singapore to challenge the long-term energy availability issues, and they propose a number of energy strategies to structure their national energy consumption and development to meeting their sustainability goals as well as the growing energy demand. The relevant policies and hydrogen developments are reviewed to illustrate utilization level of hydrogen technology.

### 3.1. Hydrogen generation

Hydrogen production is the basis for large-scale commercialization of hydrogen. At present, various hydrogen production technologies such as water electrolysis, methanol reforming, water gas, ammonia decomposition, and chlor-alkali industrial tail gas treatment have been used on a large scale. The cost of high-purity hydrogen used in fuel cells is 3–6 CNY $m^{-3}$; that is,

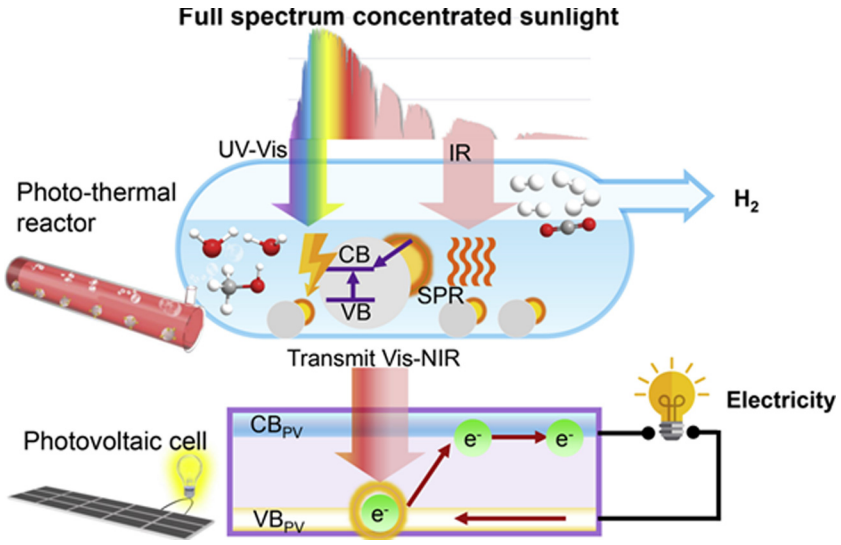


**Fig. 19.** Synergizing Concentrated Photo-Thermal Hydrogen and Photovoltaics (Tang et al., 2020).

the hydrogen consumption cost of power generation is approximately 1.7–3.4 CNY $kWh^{-1}$, which is similar to the diesel fuel consumption cost of 2.3–2.8 CNY $kWh^{-1}$.

Water electrolysis is considered as the most promising and environmentally friendly means to generate hydrogen. To solve the problem of producing silanes during the hydrolysis of $Mg_2S$, Tan et al. (2019) investigated the kinetics and mechanisms of $Mg_2Si$ hydrolysis by using $NH_4Cl$ and $NH_4F$ solution. The results showed that $NH_4F$ can nearly turn silanes into hydrogen, whereas two methods, ball milling and increasing the temperature, can both enhance the hydrogen production and hydrolysis rate. To generate hydrogen efficiently, Chen et al. studied the mechanism of Pt-$WO_3$ dual active sites, which improved hydrogen production from ammonia borane by promoting the durability and activity of the catalyst (Chen et al., 2020). Wang et al. (2016a) synthesized a catalyst for the decomposition of formic acid by preparing extra-small Pd clusters in nanosized silicalite-1 zeolite. Remarkably, the Pd $S^{-1}$-in-K catalyst offers turnover frequency values of 856 and 3027 $h^{-1}$ at 25 °C and 50 °C, respectively, owing to the Pd nanoparticle size of ∼1.5 nm.

Fuel cells can convert the energy in $H_2$ into electricity, while there are some systems that convert different power into hydrogen, and then provide reaction gas for the fuel cell to generate electricity. Photoelectrocatalytic (PEC) systems are widely used to produce renewable energy, based on photoanodes where $H_2$ is transported to generate electricity. A hybrid system synergizing photothermochemical hydrogen and photovoltaics has been designed to utilize full-spectrum sunlight efficiently to absorb ultraviolet–visible and infrared energy for rapid photothermochemical hydrogen production with Au-$TiO_2$ serving as spectrum selector (Fig. 19). (Tang et al., 2020). A Au-$TiO_2$ mixed methanol/water reaction solution serves as an absorbing selector to absorb the UV–vis/IR band for driving the hydrogen generation and to transmit the Vis–NIR band for supplying energy with the integrated PV cell, which achieved effective energy utilization. A reformer is an important device that converts hydride into hydrogen from methanol, $CH_4$, bio-oil, or even $NH_3$. For large-scale production, approximately 95% of hydrogen is produced by reforming of methane, and the remaining portions are from the electrolysis of water with the electricity generated from the combustion of fossil fuels. Hunter et al. (2016) integrated a system that can produce hydrogen from ammonia using lithium imide to power a 100 W PEMFC (Fig. 20). In their work, ammonia is passed into a cracker to generate $H_2$ and $N_2$ under purification in a reactor. They supplied a dead-ended anode operation PEMFC with the purified gas to obtain electricity to power a TV. After analysis using the Hidden Analytical HPR-20 mass spectrometer, the gas species were quantitatively certified as a mixture of composition 10% $NH_3$, 67.5% $H_2$, and 22.5% $N_2$. High-temperature fuel cells are preferred in MW-scale electricity and hydrogen production for light- and heavy-duty industry, especially solid oxide fuel cells (SOFCs) and molten carbonate fuel cell (MCFCs). A low-fuel-utilization SOFC system (Orhan and Babu, 2015) for $CO_2$-free hydrogen was exhibited by Luca et al. Their purpose was to achieve the goal of using SOFC to substitute oil refineries in $H_2$ production. However, the results showed that this system efficiency was inferior to the reference technologies; its hydrogen generation efficiency ranged from 47.1% to 60.3% and electric efficiency was between 11.6% and 19.5%. Mehdi Mehrpooya et al. (2017) designed a 6.55 MW hybrid multigeneration fuel cell system (6 MW was gained from the fuel cell and 0.55 MW from the heat recovery and steam cycle) with the function of generating gas and power containing a combined power plant, including a high-temperature fuel cell and ammonia–water absorption cycle. The synthesis gas from burning coal and oxygen was used as the primary fuel for the MCFC and hydrogen production, producing 90 kmol $h^{-1}$ hydrogen and capturing 90% of the generated $CO_2$ by a cryogenic $CO_2$ capture system. Mohammadi and Mehrpooya (2018) combined a dish collector of a solid oxide electrolyzer cell with a compressed air energy storage system including a power cycle and thermal cycle to generate hydrogen and electricity, respectively. Both thermodynamic and economic analyses were conducted, revealing that 41.48 kg $day^{-1}$ hydrogen could be produced at a normalized cost of 9.1203 \$ $kg^{-1}$ $H_2$.

There are various methods of hydrogen generation and renewable energy-driven hydrogen production technologies are promoted. Apart from the hydrogen resources, the catalysts, production efficiency, and hydrolysis rate also aspects to explore during $H_2$ generation. Moreover, fuel cell systems are becoming increasingly important in both small-scale and large-scale hydrogen generation.

### 3.2. Hydrogen storage

Generally speaking, hydrogen can be compressed ($CH_2$), liquefied ($LH_2$), or incorporated into specific storage materials (usually solid or liquid) for its later utilization in turbines, engines, high-efficiency fuel cells, or for chemicals to release its high

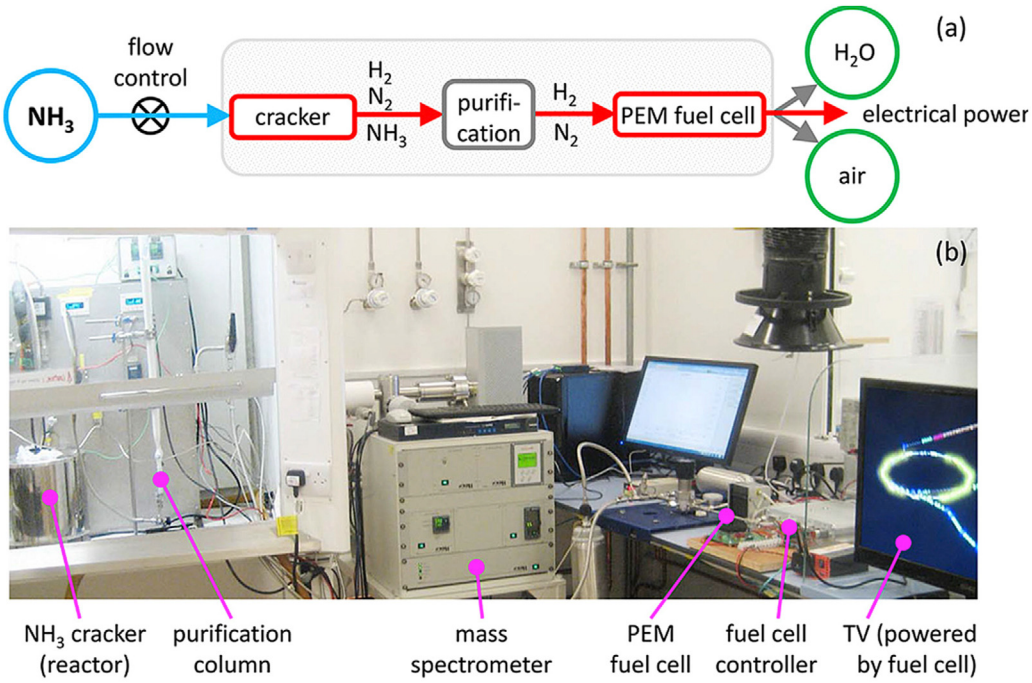


**Fig. 20.** Experimental set-up (a) system overview and (b) annotated photo.

power (Di Profio et al., 2009). Although hydrogen has many irreplaceable advantages, it still faces a great challenge in terms storage with safety, durability, and high efficiency. At present, there are three typical categories for hydrogen storage: storage in solid hydrides, gaseous storage, and liquid storage (Mellmann et al., 2016). Gaseous high-pressure hydrogen storage has the disadvantages of low hydrogen storage density and high pressure conditions, high requirements on the material of the storage device, easy leakage, and high storage cost. Metal hydride hydrogen storage has higher hydrogen storage density, better safety, and higher volume, making metal hydride more suitable for vehicle fuel cells, nickel metal hydride batteries, etc. Stored in an underground cavern or in a pressurized tank, or physically adsorbed in metals and high-surface-area adsorbents, hydrogen can be stored by physical or chemical methods. There are two reactions of dissociative chemisorption and electrochemical decomposition of water between metal and hydrogen, as shown below.

$$M + \frac{x}{2}H_2 \overset{\text{catalyst}}{\longleftrightarrow} MH_x \tag{12}$$

$$M + \frac{x}{2}H_2O + \frac{x}{2}e^- \overset{\text{catalyst}}{\longleftrightarrow} MH_x + \frac{1}{2}OH^- \tag{13}$$

Several hydrogen storage materials are characterized in Table 10. Yahya and Ismail (2018) reported the catalytic effect of $SrTiO_3$ on the hydrogen storage behavior of $MgH_2$ and found that the onset dehydrogenation temperature decreased to 275 °C. This material can take in 4.3 wt % of hydrogen in 60 min and release 5.3 wt % of hydrogen in 17 min, whereas the as-milled $MgH_2$ absorbs 1.1 wt % of hydrogen and releases 1.9 wt % of hydrogen. Tian and Shang (2019) find that by adding different types of carbon (including plasma carbon produced by plasma-reforming of hydrocarbons, activated carbon, and CNTs), the kinetics of Mg-based composites are obviously enhanced during high-energy ball milling, whereas plasma carbon shows better performance than the other two carbon structures. The milling time, amount of carbon, and carbon structure strongly influence the kinetics and de-/re-hydrogenation performance of $MgH_2$ and TiC-catalyzed $MgH_2$. Mg-based nanocomposites are stabilized and the nanoparticle growth is hindered under the influence of carbon-based nanostructures. Using X-ray diffraction (XRD), TEM, X-ray photoelectron spectroscopy (XPS), and specific surface area tests (BET), Zhao (2013) investigated the structures and hydrogen adsorption traits of Pd/MIL-101 nanocomposites and developed a 3D topology of MIL-101 before and after Pd loading in the skeleton. With Pd loading, the diffusion coefficient reached $7.233 \times 10^9$.

Liquid organic hydrogen carriers (LOHCs) offer a flexible media for the storage and transportation of hydrogen. The transportation is realized via two cycles of LOHCs, loading and unloading hydrogen into the LOHC molecule (shown in Fig. 21). Wind energy or solar energy is utilized to generate power for hydrogen production, and then by liquid H-carrier, the conversion, transportation, storage, and dehydrogenation of hydrogen are realized and can be used in applications. Di Profio et al. (2009) analyzed the energy density and storage capacity in $CGH_2$, $LG_2$, and metal hydrides. The storage capacity and energy density of $CGH_2$ (at 700 bar), $LH_2$, low-temperature metal hydrides, and high-temperature metal hydrides including the tank are 6 wt % and 0.8 kWh $L^{-1}$, 14.4 wt % and 1.1 kWh $L^{-1}$, 0.9 wt % and 3,8 kWh $L^{-1}$, and 2.9 wt % and 3.6 kWh $L^{-1}$, respectively.

Both mobile and stationary hydrogen storage have high material requirements, which is the main factor that limits their efficiency. Among the several options proposed so far, metal hydride-based solid-state storage systems have been recognized as one of the most viable solutions for storing hydrogen in hydrogen-powered systems. Most metal hydrides cannot store much hydrogen, and such hydrides have slow kinetics and do not release hydrogen at low temperatures. The main task of research in this field is to set up a metal hydride system with large hydrogen storage and kinetics at lower absorption and release temperatures.

### 3.3. Hydrogen transportation

Hydrogen delivery methods are classified into three categories according to the different states of $H_2$ during delivery: compressed gas hydrogen transportation ($CGH_2$), liquid hydrogen ($LH_2$) transportation, solid hydrogen ($SH_2$) transportation.

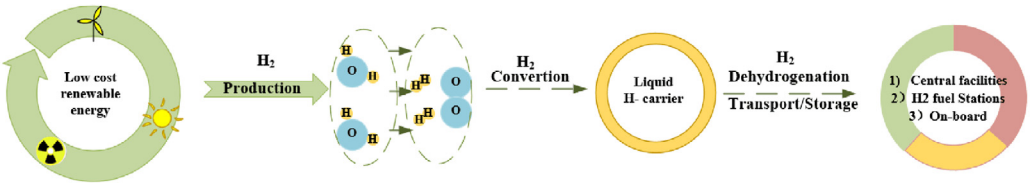


**Fig. 21.** Schematic process diagram of the role of liquid hydrogen carriers in facilitating the use of hydrogen for energy storage.

**Table 10**
Characteristics of several typical hydrogen storage materials (Di Profio et al., 2009).

| Material | Element | Hydrogen mass fraction | Advantages | Disadvantages | Representative material |
|---|---|---|---|---|---|
| Mg based alloy | Mg, Mn, Cr, Zr | 2%–7% | Large hydrogen storage mass, low cost | Low absorption rate and high releasing temperature | $Mg_2Ni$, Mg-$Li_BH_4$ |
| Rare earth alloy | La, Ni | 1.5%–2% | Large hydrogen storage mass, low cost | work at room temperature and pressure | $LaNi_5$ |
| Ti based alloy | Ti, Mn, Cr, Zr, Fe | 1.8%–4% | high absorption rate and density | high cost | FeTi |
| Zr based alloy | Zr, V, Cr, Mn | 1.4%–2.7% | Large hydrogen storage mass long lasting | Initial activation difficulty | $ZrMn_2$ |
| Organic liquid hydride | C, H | 6%-7.2% | Large hydrogen storage mass, safety | Low recycling rate of organic compounds | Benzene, Toluene, Methylcyclohexane |
| Activated carbon | C | 5%–10% | High hydrogen storage capacity, low cost, fast desorption, long cycle life and easy scale production | Low work temperature | Activated carbon |
| Carbon nanotubes | C | 2%–10% | High hydrogen storage capacity | Difficult to prepare | Carbon nanotubes |

Pipelines and trucks are the most widely used means for $H_2$ transportation, and some typical transportation methods are showed in Table 11. Zheng et al. (2019) developed a CFD model that uses a coupled level set and a fluid volume method to simulate the boiling of microgravity liquid hydrogen in a transport pipeline. The heat flux grew with the increase in gravitational acceleration; in other words, the heat flux dropped as the gravity decreased, where the reduction in heat flux could be as much as 40%. This is because as the gravity decreased, the gravitationally driven force dropped as well as the low-thermal-conductivity vapor gathered close to the heated wall. Numerical results showed that the heat flux decreased as the gravitational acceleration decreased and in the nucleating boiling state, the heat transfer rate decreased as the wall superheat increased. Ma et al. (2008) developed a hydrogen transportation cost model to calculate the large-scale cost of hydrogen transportation in Shanghai and their results revealed that the cost of $CGH_2$ by tube trailer was 2.3 CNY $kg^{-1}$, $LH_2$ by tank was 0.4 CNY $kg^{-1}$, and $GH_2$ by pipe was 6 CNY $kg^{-1}$.

### 3.4. Policy support and downstream application

#### 3.4.1. Regional organization

Regional organizations have established many roadmaps to achieve a high-efficiency, sustainable hydrogen economy, and the International Energy Agency (IEA), International Partnership, DOE, High Level Group for Hydrogen and Fuel Cells (HLG) for the Hydrogen Economy (IPHE) and others from Europe, North America, and Asia are the outstanding practitioners. IEA provides a platform to discuss common issues with energy technologies and offers opportunities for its members to keep up with these policies, and the main part of its work is hydrogen, whereas IPHE mainly focuses on international studies related to hydrogen fuel cell techniques. Both of them provide strategies, common codes, and standards to promote hydrogen development. DOE is aiming to announce its energy, environmental, and nuclear challenges through transformative science and technology. DOE has set a series of regulations to regulate hydrogen development. In 2012, DOE invested $120 million build an energy innovation hub to explore FCVs, hydrogen utilization, and wind power generation. HLG released the report "Hydrogen Energy and Fuel Cells, A vision of our future" (Höhlein, 2003) in 2003, which included the Roadmap for Europe from 2000 to 2050. An adaptation of this cycle to the HE and five proposals are highlighted, that are interconnection of local $H_2$ distribution grids, significant $H_2$ production from renewables, $H_2$ produced from fossil fuels with C sequestration, clusters of local $H_2$ distribution grids, local clusters of Hydrogen refueling stations (HRS), and local $H_2$ production at refueling station (reforming and electrolysis). In the EU, there are currently 93 HRS in operation and public accessible and in Germany alone, a $H_2$ mobility initiative network of 115 HRS was formed by 2017, and 400 are planned to be established by 2023. As many as 1180 HRS and 1.8 million hydrogen FCVs are planned in Germany for 2030 (Wang et al., 2016b).

#### 3.4.2. National strategy

As shown in Figs. 1–4, many countries have developed their domestic roadmap for hydrogen and fuel cells. Many countries incorporate hydrogen development in their national strategies and implement numerous measures to promote it. The Japanese government has elevated hydrogen energy to a national strategy with a mature industrial chain leading in technology and commercialization. By this domestic concentration, Japan has made great progress, with a production capacity of over 10,000 units of Toyota Mirai, more than 300,000 sets of Ene-farm cogeneration system, and more than 100 HRSs. In order to improve China's fuel cell industry chain technology, the government attaches numerous elements of financial and political support to the hydrogen energy industry and proposes a government work report to promote the construction of hydrogenation facilities. By 2019, the nationalization level of China's power reactor industry chain reached 50%, and the localization of key components of the system reached 70%. Commercial vehicles are the mainstay

**Table 11**
Comparison of hydrogen transportation methods.

| # | $H_2$ state | Traffic volume | Application | Character |
|---|---|---|---|---|
| Assembly grid | $CGH_2$ | 5–10 kg/grid | Commercial hydrogen transportation | Mature technology, small traffic volume |
| Compressed gas truck (tube trailer) | $CGH_2$ | 250–460 kg | Commercial hydrogen transportation | large traffic volume, but unfit for long distance transportation |
| Pipe | $CGH_2$ | 310–8,900 kg $h^{-1}$ | Chemical plant | large traffic volume and high delivery efficiency, but high first investment cost |
| Tank truck | $LH_2$ | 360–4 300 kg $car^{-1}$ | Widely used abroad, domestically only used for aerospace liquid hydrogen transport | large traffic volume, but high request for devices and high cost for liquation and energy consumption. |
| Railway | $LH_2$ | 2,300–9,100 kg $car^{-1}$ | Less used abroad, no used domestic | large traffic volume |

in the early days of China's fuel cell development and FCVs as well as HRSs in China now number more than 4500 and 20, respectively. One million FCVs and 1000 HRSs are planned to be established by 2030. Korea has strong support, high subsidies, and a relatively mature industrial chain for fuel cells. In 2018, South Korea operated 889 FCVs, 14 HRSs, and the installed capacity of power stations reached 307 MW. It plans to have 2.9 million fuel cell vehicles, 1200 HRSs, and 15 GW of power stations by 2040. The US DOE launched the National Hydrogen Energy Development Prospects and Guidelines Project. According to the US Hydrogen Energy Technology Roadmap, that nation will enter the era of the "hydrogen energy economy" by 2040. A wind energy hydrogen-based energy application demonstration project was also launched by DOE, established on Long Island, New York, which uses wind turbines to supply electricity to a water electrolysis hydrogen conversion process. The hydrogen produced is stored in the hydrogen station of Long Island, and used for fuel cell vehicles in that region. In addition, the DOE also carried out the world's largest demonstration of fuel cell vehicles, including 183 FCVs and 25 HRSs, driving a total of 3.6 million miles.

Apart from China, Asian countries, such as Japan, Korea, India, and Malaysia, are participating in an active discussion on the hydrogen economy. Hydrogen and fuel cells are included in the development plan of China, the National Medium and Long-Term Science and Technology Development Plan (2006–2020), and a clear objective has been set. In 2030, the hydrogen energy industry will become an essential part of China's new economic growth point and new energy strategy. Japan has been planning and developing hydrogen technology for a long time and has achieved numerous breakthroughs, and these advances can be credited to its continuous investment in the hydrogen industry. In 2004, 31 billion yen (Behling et al., 2015) was utilized by the Japanese government for research and development of fuel cells. Additionally, $4 billion has been used for hydrogen usage in fuel cells for vehicles and stationary applications and by 2020, all road vehicles are expected to be powered by hydrogen-based fuel cells. The Japanese government also directed resources to support Japanese automakers and invest approximately $380 million per year on research, progress, and commercialization of fuel cells. The Korean government has already allocated $38 million as an additional budget to develop a greener renewable hydrogen economy. A report by Tak (2010) in 2010 showed that $90 million per year was invested by the Korean government for the research and development of hydrogen and fuel cells.

### 3.4.3. Commercial application

Generally, hydrogen is primarily used in petroleum refining, ammonia production, metal refining, and other downstream applications, such as internal combustion engines (ICEs) and turbines, apart from FCVs (as shown in Fig. 22). For ICEs, biodiesel and hydrogen are used as test fuels in the experimental investigations during the dual fuel operation of a diesel engine (Verma et al., 2019). By using a hydrogen injector and electronic control unit, the main fuel, hydrogen, was injected in the intake manifold. It was found that in comparison with single-fuel diesel engine operation, this dual-fuel engine could consume up to 80.7% and 24.5% hydrogen at low and high loading respectively, with a significant reduction in the smoke emissions of hydrocarbons and carbon monoxide. Hydrogen turbines are widely utilized to raise the pressure of hydrogen-rich streams in refineries to satisfy the operating pressure requirements of various hydrogenation units. Fuel cells are ready for commercial leasing and selling in certain major automotive companies, such as Toyota, Honda, and Hyundai, introduced in detail in this review. Additionally, some top companies, such as Walmart, Whole Foods, Coca-Cola, and FedEx, are using fuel cells to supply power (Singh et al., 2008). For chemicals, hydrogen is primarily utilized for producing ammonia and other chemicals in the petrochemical industry. A report (Balat, 2008) revealed that out of a total of 500 billion cubic meters ($Bm^3$) of hydrogen, ammonia production, other chemical products, and petrochemistry accounted for 50% (250 $Bm^3$), 13% (65 $Bm^3$), and 37% (185 $Bm^3$), respectively.

Component manufacturing is the highlight in fuel cell commercial application, and Ballard, LCS, Toyota, and SRM are the major component suppliers in the world. There are some companies that provide the mature design, development, production, and service of PEMFCs, such as Ballard, Plug Power, and Hydrogenics Corporation, and the product of the latter, called HyPM, can output 1 KW–1 GW electricity. Bloom Energy and UTC Power once worked for NASA for energy supply of spacecraft, and are now focusing on the development of SOFCs to provide electricity in microhousehold fuel cells by using their marquee products, Bloom Box and Pure Cell, respectively. Fuel Cell Energy is mainly engaged in the research of stationary fuel cells and its main products are MCFCs for on-site power generation, cogeneration, and distributed generation used in the power industry, business and enterprise, government agencies, and so on. The company's current DFC power plant has produced ultraclean, efficient, and reliable power in more than 50 locations worldwide, with the ability to produce more than 1.5 billion kWh of ultraclean power and more than 300 MW of generating capacity. In October 2009, Toshiba released a direct methanol fuel cell (DMFC) called Dynario in Japan, which automatically generates electricity as long as methanol is fed into the unit. The power generated can be

**Table 12**
Selected emission reduction goals of participating regions and cities (Anon, 2018a).

| City | London | Torres Vedras | Aberdeen | Oslo | Riga | Hamburg | Venice | Pays de la Loire |
|---|---|---|---|---|---|---|---|---|
| Goal | Be a zero carbon city by 2050 | Reduce $CO_2$ emissions by 29% by 2020 | Reduce carbon emissions by at least 50% by 2030 | Reduce climate emissions by 95% by 2030 | Reduce $CO_2$ emissions by 55% by 2020 | Reduce $CO_2$ emissions by 40% by 2020 | Reduce $CO_2$ emissions by 20% by 2020 | Reduce $CO_2$ emissions by 23% by 2020 |

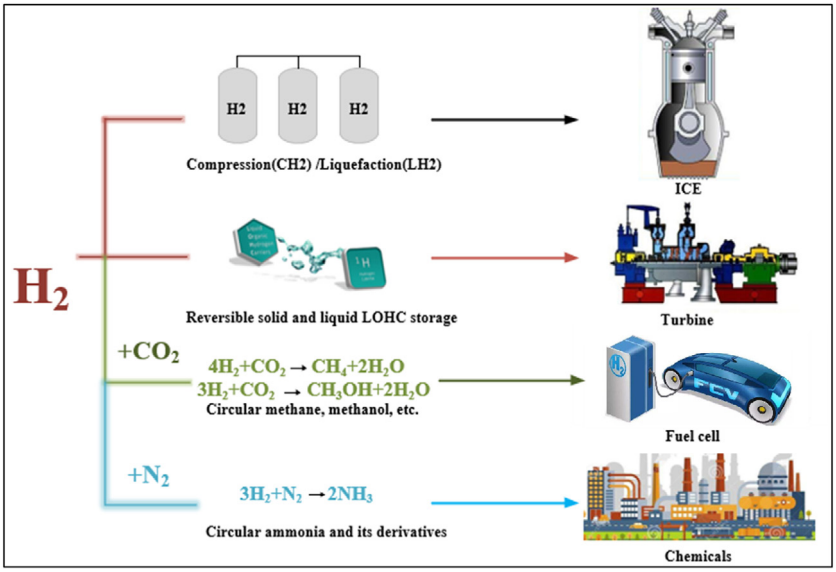


**Fig. 22.** Utilization of the renewable energy through hydrogen storage pathways.

used to charge a built-in lithium-ion battery or provide a DC 5 V output via a USB interface; however, the Dynario provides a slightly smaller current of 400 mA. The Dynario machine itself has 14 ml of methanol content, which can provide sufficient power to charge two mobile phones. The UK's ITM Energy Company implemented a hydrogen energy demonstration project in the Rotherham area of the UK to provide partial power support and hydrogen fuel for nearby buildings. The system consists of a 225 kW wind turbine, an advanced electrolysis cell, a hydrogen storage system for storing 200 kg of hydrogen, and a fuel cell power system with a power of 30 kW. The hydrogen energy integrated demonstration system combines ITM Energy's most advanced hydrogen energy commercialization module and is a very important component of the UK's hydrogen energy infrastructure. Sweden's Vatten Fall has established Europe's first hydrogen–wind energy renewable energy power plant, which uses wind energy to produce hydrogen. Taking China as an example to introduce component production, stack companies are supported by independent research and development and technology introduction, such as Guangdong Guorui, Weichai. MEA, PEM, and BP can be mass-produced, whereas the catalyst and GDL can only be produced at small scales. University related high-tech enterprises are the main force for these productions, such as Dongyue or Wuhan University of Science and Technology.

### *3.4.4. Typical application*

Fuel cells and hydrogen (FCH) technology can be a key enabler to reduce emissions and realize the green energy transition. While governments are providing comparatively easy-to-control reductions owing to the domestic energy policies and uptake of renewable, some cities have launched pilot programs to start the hydrogen applications supported by their governments. With a history of more than 200 years, the UK gas industry is spread over the whole country and forms a national gas network, and now more than 80% of its population uses the gas network for fundamental cooking and heating. Although natural gas, the lowest-carbon-dioxide-releasing fossil fuel per unit energy, produces approximately 180 g $kWh^{-1}$ $CO_2$, hydrogen produces zero $CO_2$ emissions. It is possible for the existing natural gas network to be converted into a hydrogen network by zone division (funded by UK government) incrementally through summer months over a three-year period, implying minimal disruption for customers during the conversion and negligible impact on customer total gas bills.

The H21 Leeds City Gate Project (Anon, 2016c), as shown in Fig. 23, is a study funded by the UK Government that focuses on assessing, from both a technical and economic perspective, the feasibility of converting the existing methane gas network in Leeds to a 100% hydrogen gas network. As the report shows, the maximum peak hour demand for Section 2 is 3180 MW (NGN1 in 20 peak hour demand). Steam methane reformers (SMRs) and a seasonal salt cavern storage located in Teesside are connected by a hydrogen transmission system (HTS) to the area of conversion (Leeds), and the hydrogen production capacity is more than the peak supply requirement of 3180 MW. The carbon capture method toward compressing $CO_2$ to 140 bar and sequestration deep under the North Sea is well established alongside the SMR operations. For the UK carbon budget basis, compared to using natural gas (184 g $kWh^{-1}$), hydrogen (27 g $kWh^{-1}$) will reduce 85% of $CO_2$ emissions, which implies that 1.5 million tons of $CO_2$ per annum would be sequestered by this project.

Regions and cities can benefit from investing in hydrogen and fuel cells not only in environmental terms, but also by providing a reliable and efficient supply of green energy to stimulate local economic growth, which is why a board range of applications of hydrogen and fuel cells are ready to be deployed for all energy and transport sectors. Most participants have developed their own strategies (as shown in Table 12), including a long-term vision for local energy transition, in which hydrogen and fuel cells play an important role in their future energy systems (Anon, 2018a).

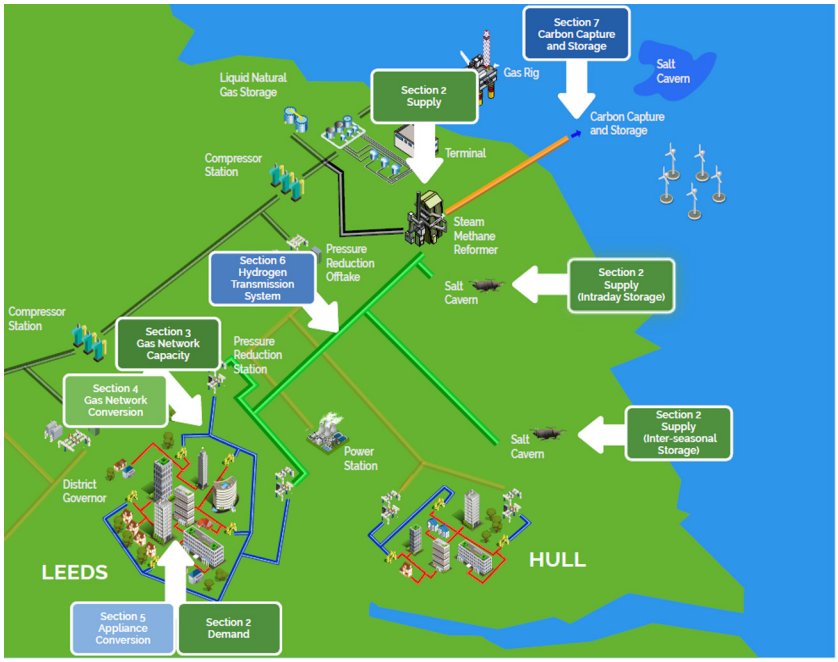


**Fig. 23.** H21 Leeds City Gate System Schematic (Anon, 2016c).

## 4. Conclusion

In the coming decades, to prevent environmental degradation and reduce dependence on fossil fuels, humans are expected to increasingly use clean energy, specifically hydrogen energy. Hydrogen is likely to play a key role alongside electrification in decarbonizing global energy systems. The high volumetric hydrogen density and ease of storage and transportation make liquid hydrogen-containing carriers attractive for reducing the infrastructure burden of implementation. Three main conclusions are drawn after reviewing related papers, covering the fuel cell design, commercial markets, as well as strategy support.

(1) Stability and cost are still the main challenges in commercial releasing, which requires the technical support for large-scale, low-cost, and stable applications. Material, structural design, and system integration are the three key factors limiting the energy improvement and technological advancement. The structure of fuel cells should be designed to perform more efficiently, and hydrogen technologies in generation and storage must focus on achieving the material advancements for the development of its safety and stability during operation. Systems should be properly designed to link between hydrogen production, storage, transportation, and utilization with durability and high efficiency.

(2) Unlike fuel vehicles, zero emission could be the most attractive aspect of the commercial FCV market. In comparison with the electric vehicles, the driving range and refueling time are the advantages of FCV for buses and heavy trucks. Therefore, it is foreseeable that FCVs have a wide application in the transportation field among cities, railways, seaports, and warehouses. The FCV is a promising substitute for fuel vehicles, and thus this fuel cell integration system should set the target on lowering cost, promoting stability and performance, and installing HRSs, which can help it capture market share in the recent vehicle market.

(3) Successful applications need more powerful, focused, and long-term energy strategies and public policies with great pressure on challenging the traditional energy system, requiring low-carbon technology innovation. Regional coordination organization should make proper policies considering the imbalance between different countries, and offer support and guide countries in hydrogen policy-making. For a country, a fully developed policy system should be founded in advance to support the innovation and development of hydrogen and fuel cell technology that provides the stability and vitality to satisfy feasible and reasonable performance and cost targets.

## Declaration of competing interest

The authors declare that they have no known competing financial interests or personal relationships that could have appeared to influence the work reported in this paper.

## Acknowledgments

This work is supported by the National Key Research and Development Program of China (No. 2018YFC0810000), the National Natural Science Foundation of China (No. 51776144), the Natural Science Foundation of Hubei Province (No. 2020CFA040), Wuhan Applied Foundational Frontier Project (No. 2020010601012205) and the Fundamental Research Funds for the Central Universities (No. 2019kfyRCPY09).

## References

A, M.G., 2001. Thin graphite bipolar plate with associatedgaskets and carbon cloth flow field for use in an ionomer membranefuel cell US.
Adamson, K.A., Butler, J., Hugh, M., 2008. Fuel cell today industry review 2008: Fuel cells: Commercialisation. Platinum Met. Rev. 52 (2), 123.
Afra, M., Nazari, M., Kayhani, M.H., Sharifpur, M., Meyer, J.P., 2019. 3D experimental visualization of water flooding in proton exchange membrane fuel cells. Energy 175, 967–977.
America, H.M., 2015. Hyundai tucson fuel cell.
Anon, 2014a. Golf SportswagenHymotion makes global debut at the 2014 los angeles auto show.
Anon, 2014b. Honda's FCV concept brings 'Clarity' back into the fuel cell fold.
Anon, 2014c. The VW golf SportWagenHyMotion may be the most advanced golf yet.
Anon, 2015a. The 13th five-year plan in China.
Anon, 2015b. Audi makes fuel cells look good with the A7 sportback h-tron.
Anon, 2015c. Honda FCV concept.
Anon, 2016a. Hydrogen Fuel Stations in California: A Practical Guide to Permitting and CEQR Review. Arnold and Porter LLP.
Anon, 2016b. The audi A7 sportback h tronquattro.

Anon, 2016c. H21 leeds city gate executive summry.
Anon, 2016d. Toyota FCHV hydrogen hybrid vehicle.
Anon, 2017. The strategic roadmap for hydrogen and fuel cells in Japan.
Anon, 2018a. Fuel Cell and Hydrogen for Green Energy in European Cities and Regions :FUCJU Regions Cities Final Report.
Anon, 2018b. Hydrogen roadmap Korea:A vision, roadmap and recommendation to develop Korea's hydrogen economy.
Anon, 2018c. Japan H2 mobility to accelerate deployment of hydrogen stations. Fuel Cell Bull. 9.
Anon, 2019. Hydrogen roadmap Europe: A sustainable pathway for the European energy transition.
Arruda, B.A., Santos, M.M., Keshri, R.K., Ieee, 2016. A comparative study of performance for electric vehicles for wheel traction configurations. In: Proceedings 2016 Ieee 25th International Symposium on Industrial Electronics. Ieee, New York, pp. 786–792.
Balat, M., 2008. Potential importance of hydrogen as a future solution to environmental and transportation problems. Int. J. Hydrogen Energy 33, 4013–4029.
Behling, N., Williams, M.C., Managi, S., 2015. Fuel cells and the hydrogen revolution: Analysis of a strategic plan in Japan. Econ. Anal. Policy 48, 204–221.
Boillat, P., Kramer, D., Seyfang, B.C., Frei, G., Lehmann, E., Scherer, G.G., Wokaun, A., Ichikawa, Y., Tasaki, Y., Shinohara, K., 2008. In situ observation of the water distribution across a PEFC using high resolution neutron radiography. Electrochem. Commun. 10, 546–550.
Brey, J.J., Carazo, A.F., Brey, R., 2018. Exploring the marketability of fuel cell electric vehicles in terms of infrastructure and hydrogen costs in Spain. Renew. Sustain. Energy Rev. 82, 2893–2899.
Chen, W., Fu, W., Qian, G., Zhang, B., Chen, D., Duan, X., Zhou, X., 2020. Synergistic Pt-WO3 dual active sites to boost hydrogen production from ammonia borane. iScience 23, 100922.
Chen, B., Wang, M., Tu, Z., Gong, X., Zhang, H., Pan, M., Cai, Y., Wan, Z., 2015. Moisture dehumidification and its application to a 3 kW proton exchange membrane fuel cell stack. Int. J. Hydrogen Energy 40, 1137–1144.
Chini, M.E., Fabrizio, K. Manfred, 2019. Bipolar plate, US.
Das, H.S., Tan, C.W., Yatim, A.H.M., 2017. Fuel cell hybrid electric vehicles: A review on power conditioning units and topologies. Renew. Sustain. Energy Rev. 76, 268–291.
Debe, M., 2013. Tutorial on the fundamental characteristics and practical properties of nanostructured thin film (NSTF) catalysts. J. Electrochem. Soc. 160, F522–F534.
Demirbas, A., 2005. Hydrogen and boron as recent alter native motor fuels. Energy Sources A 27, 7–41.
Di Profio, P., Arca, S., Rossi, F., Filipponi, M., 2009. Comparison of hydrogen hydrates with existing hydrogen storage technologies: Energetic and economic evaluations. Int. J. Hydrogen Energy 34, 9173–9180.
Ding, J., Wang, P., Ji, S., Wang, H., Linkov, V., Wang, R., 2019. N-doped mesoporous FeNx/carbon as ORR and OER bifunctional electrocatalyst for rechargeable zinc-air batteries. Electrochim. Acta 296, 653–661.
Energy, D.o., 2016. Department of energy US. Vehicles and manufacturers.
Fabian, T., O'Hayre, R., Litster, S., Prinz, F., Santiago, J., 2006. Water management at the cathode of a planar air-breathing fuel cell with an electroosmotic pump. ECS Trans. 3.
Garapati, M.S., Sundara, R., 2019. Highly efficient and ORR active platinum-scandium alloy-partially exfoliated carbon nanotubes electrocatalyst for Proton Exchange Membrane Fuel Cell. Int. J. Hydrogen Energy 44, 10951–10963.
Gherairi, S., 2019. Hybrid electric vehicle: Design and control of a hybrid system (Fuel cell/battery/ultra-capacitor) supplied by hydrogen. Energies 12, 19.
Haragirimana, A., Ingabire, P.B., Zhu, Y., Lu, Y., Li, N., Hu, Z., Chen, S., 2019. Four-polymer blend proton exchange membranes derived from sulfonated poly(aryl ether sulfone)s with various sulfonation degrees for application in fuel cells. J. Membr. Sci. 583, 209–219.
Hassan, N.S.M., Daud, W.R.W., Sopian, K., Sahari, J., 2009. Water management in a single cell proton exchange membrane fuel cells with a serpentine flow field. J. Power Sources 193, 249–257.
Hezarjaribi, M., Jahanshahi, M., Rahimpour, A., Yaldagard, M., 2014. Gas diffusion electrode based on electrospun Pani/CNF nanofibers hybrid for proton exchange membrane fuel cells (PEMFC) applications. Appl. Surf. Sci. 295, 144–149.
Höhlein, B., 2003. Hydrogen and fuel cells - a vision of our future.
Holloway, H., 2015. Japan pushes hydrogen infrastructure.
Huang, H.-j., Yang, T., Lai, F.-y., Wu, G.-q., 2017. Co-pyrolysis of sewage sludge and sawdust/rice straw for the production of biochar. J. Anal. Appl. Pyrolysis 125, 61–68.
Hunter, H.M.A., Makepeace, J.W., Wood, T.J., Mylius, O.S., Kibble, M.G., Nutter, J.B., Jones, M.O., David, W.I.F., 2016. Demonstrating hydrogen production from ammonia using lithium imide – Powering a small proton exchange membrane fuel cell. J. Power Sources 329, 138–147.
Ijaodola, O.S., El-Hassan, Z., Ogungbemi, E., Khatib, F.N., Wilberforce, T., Thompson, J., Olabi, A.G., 2019. Energy efficiency improvements by investigating the water flooding management on proton exchange membrane fuel cell (PEMFC). Energy 179, 246–267.
Iyuke, S.E., Mohamad, A.B., Kadhum, A.A.H., Daud, W.R.W., Rachid, C., 2003. Improved membrane and electrode assemblies for proton exchange membrane fuel cells. J. Power Sources 114, 195–202.
Kahraman, H., Orhan, M.F., 2017. Flow field bipolar plates in a proton exchange membrane fuel cell: Analysis & modeling. Energy Convers. Manage. 133, 363–384.
Kendall, M., 2018. Fuel cell development for new energy vehicles (NEVs) and clean air in China. Prog. Nat. Sci. Mater. Int. 28, 113–120.
Kim, J.-H., Kim, H.-J., Yoo, S.-H., 2019. Willingness to pay for fuel-cell electric vehicles in South Korea. Energy 174, 497–502.
Kirk, B.W., 1994. Laminated fluid flow field assembly for electrochemicalfuelcells, US.
Kusoglu, A., Weber, A.Z., 2017. New insights into perfluorinated sulfonic-acid ionomers. Chem. Rev. 117, 987–1104.
Lattin, W.C., Utgikar, V.P., 2006. Transition to hydrogen economy in the United States: A 2006 status report. Int. J. Hydrogen Energy 32, 3230–3237.
Lee, D., Bae, J., 2012. Visualization of flooding in a single cell and stacks by using a newly-designed transparent PEMFC. Int. J. Hydrogen Energy 37, 422–435.
Lin, S.-Y., Chang, M.-H., 2015. Effect of microporous layer composed of carbon nanotube and acetylene black on polymer electrolyte membrane fuel cell performance. Int. J. Hydrogen Energy 40, 7879–7885.
Lin, J.F., Wertz, J., Ahmad, R., Thommes, M., Kannan, A.M., 2010. Effect of carbon paper substrate of the gas diffusion layer on the performance of proton exchange membrane fuel cell. Electrochim. Acta 55, 2746–2751.
Litster, S., McLean, G., 2004. PEM fuel cell electrodes. J. Power Sources 130, 61–76.
Liu, K., Qiao, Z., Hwang, S., Liu, Z., Zhang, H., Su, D., Xu, H., Wu, G., Wang, G., 2019. Mn- and N- doped carbon as promising catalysts for oxygen reduction reaction: Theoretical prediction and experimental validation. Appl. Catal. B 243, 195–203.
Ma, J., Liu, S., Zhou, W., Pan, X., 2008. Comparison of hydrogen transportation methods for hydrogen refueling station. Tongji Daxue Xuebao/J. Tongji Univ. 36, 615–619.
Mahjoubi, C., Olivier, J.-C., Skander-mustapha, S., Machmoum, M., Slama-belkhodja, I., 2019. An improved thermal control of open cathode proton exchange membrane fuel cell. Int. J. Hydrogen Energy 44, 11332–11345.
Mahlou, S.W., 1998. Fuel cell with metal screen flow field, US.
Majlan, E.H., Rohendi, D., Daud, W.R.W., Husaini, T., Haque, M.A., 2018. Electrode for proton exchange membrane fuel cells: A review. Renew. Sustain. Energy Rev. 89, 117–134.
Manoharan, Y., Hosseini, S.E., Butler, B., Alzhahrani, H., Fou, B.T., Ashuri, T., Krohn, J., 2019. Hydrogen fuel cell vehicles; current status and future prospect. Appl. Sci.-Basel 9, 17.
Mehrpooya, M., Rahbari, C., Moosavian, S.M.A., 2017. Introducing a hybrid multi-generation fuel cell system, hydrogen production and cryogenic $CO_2$ capturing process. Chem. Eng. Process. Process Intensif. 120, 134–147.
Mellmann, D., Sponholz, P., Junge, H., Beller, M., 2016. Formic acid as a hydrogen storage material - development of homogeneous catalysts for selective hydrogen release. Chem. Soc. Rev. 45, 3954–3988.
MERCURI, R.A., IIILLS, S., GOUGH, J.J., 2000. Flexible graphitecomposite for use in the form of a fuel cell flow field plate, US.
Middelman, E., 2002. Improved PEM fuel cell electrodes by controlled self-assembly. Fuel Cells Bull. 2002, 9–12.
Mohammadi, A., Mehrpooya, M., 2018. Techno-economic analysis of hydrogen production by solid oxide electrolyzer coupled with dish collector. Energy Convers. Manage. 173, 167–178.
Mosdale, R., Srinivasan, S., 1995. Analysis of performance and of water and thermal management in proton exchange membrane fuel cells. Electrochim. Acta 40, 413–421.
Murata, S., Imanishi, M., Hasegawa, S., Namba, R., 2014. Vertically aligned carbon nanotube electrodes for high current density operating proton exchange membrane fuel cells. J. Power Sources 253, 104–113.
Neethu, B., Bhowmick, G.D., Ghangrekar, M.M., 2019. A novel proton exchange membrane developed from clay and activated carbon derived from coconut shell for application in microbial fuel cell. Biochem. Eng. J. 148, 170–177.
Nikiforow, K., Ihonen, J., Keränen, T., Karimäki, H., Alopaeus, V., 2014. Modeling and experimental validation of $H_2$ gas bubble humidifier for a 50 kW stationary PEMFC system. Int. J. Hydrogen Energy 39, 9768–9781.
Nonobe, Y., 2017. Development of the fuel cell vehicle mirai. IEEJ Trans. Electr. Electron. Eng. 12, 5–9.
Oh, K., Kwon, O., Son, B., Lee, D.H., Shanmugam, S., 2019. Nafion-sulfonated silica composite membrane for proton exchange membrane fuel cells under operating low humidity condition. J. Membr. Sci. 583, 103–109.
Oh, H.-S., Oh, J.-G., Haam, S., Arunabha, K., Roh, B., Hwang, I., Kim, H., 2008. On-line mass spectrometry study of carbon corrosion in polymer electrolyte membrane fuel cells. Electrochem. Commun. 10, 1048–1051.

Orhan, M.F., Babu, B.S., 2015. Investigation of an integrated hydrogen production system based on nuclear and renewable energy sources: Comparative evaluation of hydrogen production options with a regenerative fuel cell system. Energy 88, 801–820.
Park, Y.H., Caton, J.A., 2008. An experimental investigation of electro-osmotic drag coefficients in a polymer electrolyte membrane fuel cell. Int. J. Hydrogen Energy 33, 7513–7520.
Paul, M.T.Y., Saha, M.S., Qi, W.L., Stumper, J., Gates, B.D., 2019. Microstructured membranes for improving transport resistances in proton exchange membrane fuel cells. Int. J. Hydrogen Energy.
Pillai, S.R., Sonawane, S.H., Gumfekar, S.P., Suryawanshi, P.L., Ashokkumar, M., Potoroko, I., 2019. Continuous flow synthesis of nanostructured bimetallic Pt-Mo/C catalysts in milli-channel reactor for PEM fuel cell application. Mater. Chem. Phys. 237, 121854.
Qiang, M.Z., 2005. Hydrogen: Green Energy in the 21st Century. Chemical Industry Press, Beijing.
Qu, L., Wang, Z., Guo, X., Song, W., Xie, F., He, L., Shao, Z., Yi, B., 2019. Effect of electrode Pt-loading and cathode flow-field plate type on the degradation of PEMFC. J. Energy Chem. 35, 95–103.
Rahimi-Esbo, M., Ramiar, A., Ranjbar, A.A., Alizadeh, E., 2017. Design, manufacturing, assembling and testing of a transparent PEM fuel cell for investigation of water management and contact resistance at dead-end mode. Int. J. Hydrogen Energy 42, 11673–11688.
Ralph, T.R., Hards, G.A., Keating, J.E., Campbell, S.A., Wilkinson, D.P., Davis, M., St-Pierre, J., Johnson, M.C., 1998. ChemInform abstract: Low cost electrodes for proton exchange membrane fuel cells. Performance in single cells and ballard stacks. ChemInform 29.
Reiser, C.A., Sawyer, R.D., 1988. Solid polymer electrolyte fuel cell stack water management system, US.
Samad, S., Loh, K.S., Wong, W.Y., Lee, T.K., Sunarso, J., Chong, S.T., Wan Daud, W.R., 2018. Carbon and non-carbon support materials for platinum-based catalysts in fuel cells. Int. J. Hydrogen Energy 43, 7823–7854.
Sasabe, T., Tsushima, S., Hirai, S., 2010. In-situ visualization of liquid water in an operating PEMFC by soft X-ray radiography. Int. J. Hydrogen Energy 35, 11119–11128.
Schwelm, G., 2009. Hydrogenics fueling installations in Germany. Fuel Cells Bull. 7.
Scofield, M., Liu, H., Wong, S., 2015. A concise guide to sustainable PEMFCs: recent advances in improving both oxygen reduction catalysts and proton exchange membranes. Chem. Soc. Rev. 44.
Shen, J., Tu, Z., Chan, S.H., 2020. Performance enhancement in a proton exchange membrane fuel cell with a novel 3D flow field. Appl. Therm. Eng. 164, 114464.
Shim, J.Y., Tsushima, S., Hirai, S., 2009. High resolution MRI investigation of transversal water content distributions in PEM under fuel cell operation. ECS Trans. 523–528.
Singh, R., Gupta, N., Poole, K.F., 2008. Global green energy conversion revolution in 21st century through solid state devices. In: 2008 26th International Conference on Microelectronics, pp. 45–54.
Sitanggang, R., Mohamad, A.B., Daud, W.R.W., Kadhum, A.A.H., Iyuke, S.E., 2009. Fabrication of gas diffusion layer based on x–y robotic spraying technique for proton exchange membrane fuel cell application. Energy Convers. Manage. 50, 1419–1425.
Sprik, S., Kurtz, J., Ainscough, C., Saur, G., Peters, M., 2015. Hydrogen station data collection and analysis: 2015 annual merit review. In: Proceedings of DOE annual merit review meeting, Washington DC, USA.
Srinivasan, V., Higuchi, W.I., Su, M.-H., 1989. Baseline studies with the four-electrode system: The effect of skin permeability increase and water transport on the flux of a model uncharged solute during iontophoresis. J. Control. Release 10, 157–165.
Strahl, S., Costa-Castelló, R., 2016. Model-based analysis for the thermal management of open-cathode proton exchange membrane fuel cell systems concerning efficiency and stability. J. Process Control 47, 201–212.
Su, H., Pasupathi, S., Bladergroen, B., Linkov, V., Pollet, B.G., 2013. Optimization of gas diffusion electrode for polybenzimidazole-based high temperature proton exchange membrane fuel cell: Evaluation of polymer binders in catalyst layer. Int. J. Hydrogen Energy 38, 11370–11378.
Sulaiman, N., Hannan, M.A., Mohamed, A., Majlan, E.H., Wan Daud, W.R., 2015. A review on energy management system for fuel cell hybrid electric vehicle: Issues and challenges. Renew. Sustain. Energy Rev. 52, 802–814.
Sutradhar, S.C., Rahman, M.M., Ahmed, F., Ryu, T., Yoon, S., Lee, S., Kim, J., Lee, Y., Jin, Y., Kim, W., 2019. Thermally and chemically stable poly(phenylenebenzophenone) membranes for proton exchange membrane fuel cells by Ni (0) catalyst. J. Ind. Eng. Chem. 76, 233–239.
Tak, Y., 2010. National program of hydrogen and fuel cells in Korea, on behalf of ministry of knowledge economy.
Tan, Z.H., Ouyang, L.Z., Huang, J.M., Liu, J.W., Wang, H., Shao, H.Y., Zhu, M., 2019. Hydrogen generation via hydrolysis of $Mg_2Si$. J. Alloys Compd. 770, 108–115.
Tanç, B., Arat, H.T., Baltacıoğlu, E., Aydın, K., 2019. Overview of the next quarter century vision of hydrogen fuel cell electric vehicles. Int. J. Hydrogen Energy 44, 10120–10128.
Tang, S., Xing, X., Yu, W., Sun, J., Xuan, Y., Wang, L., Xu, Y., Hong, H., Jin, H., 2020. Synergizing photo-thermal H2 and photovoltaics into a concentrated sunlight use. iScience 23, 101012.
Teixeira, F.C., de Sá, A.I., Teixeira, A.P.S., Rangel, C.M., 2019. Nafion phosphonic acid composite membranes for proton exchange membranes fuel cells. Appl. Surf. Sci. 487, 889–897.
Tian, M., Shang, C., 2019. Mg-based composites for enhanced hydrogen storage performance. Int. J. Hydrogen Energy 44, 338–344.
Tüber, K., Pócza, D., Hebling, C., 2003. Visualization of water buildup in the cathode of a transparent PEM fuel cell. J. Power Sources 124, 403–414.
Van Dao, D., Adilbish, G., Lee, I.-H., Yu, Y.-T., 2019. Enhanced electrocatalytic property of Pt/C electrode with double catalyst layers for PEMFC. Int. J. Hydrogen Energy 44, 24580–24590.
Verma, S., Suman, A., Das, L.M., Kaushik, S.C., Tyagi, S.K., 2019. A renewable pathway towards increased utilization of hydrogen in diesel engines. Int. J. Hydrogen Energy.
VorsprungdurchTechnik, A., 2015. Audi A7 sportback h-tronquattro.
Voss, H.H., Chow, C.Y., 1993. Coolant flow field plate for electrochemical fuel cells, US.
W, D.P., 1996. Embossed fluid flow field plate for electrochemical fuelcell, US.
Wakita, H., Kawabata, N., Kani, Y., 2019. Measurement of water permeation through membranes from extremely high hydraulic pressure to atmospheric pressure. Int. J. Hydrogen Energy 44, 31257–31262.
Wang, J., Li, P., Zhang, Y., Liu, Y., Wu, W., Liu, J., 2019a. Porous nafion nanofiber composite membrane with vertical pathways for efficient through-plane proton conduction. J. Membr. Sci. 585, 157–165.
Wang, Y., Moura, S.J., Advani, S.G., Prasad, A.K., 2019b. Power management system for a fuel cell/battery hybrid vehicle incorporating fuel cell and battery degradation. Int. J. Hydrogen Energy 44, 8479–8492.
Wang, N., Qiming, S., Bai, R., Li, X., Guo, G., Yu, J., 2016a. In situ confinement of ultra-small Pd clusters within nanosized silicalite-1 zeolite for high-efficient hydrogen generation catalysis. J. Am. Chem. Soc. 138.
Wang, Y., Ruiz Diaz, D.F., Chen, K.S., Wang, Z., Adroher, X.C., 2020. Materials, technological status, and fundamentals of PEM fuel cells – A review. Mater. Today 32, 178–203.
Wang, E.-D., Shi, P.-F., Du, C.-Y., 2008. Treatment and characterization of gas diffusion layers by sucrose carbonization for PEMFC applications. Electrochem. Commun. 10, 555–558.
Wang, N., Sun, Q., Bai, R., Li, X., Guo, G., Yu, J., 2016b. In situ confinement of ultrasmall Pd clusters within nanosized silicalite-1 zeolite for highly efficient catalysis of hydrogen generation si.
Wang, R., Zhang, G., Hou, Z., Wang, K., Zhao, Y., Jiao, K., 2019c. Comfort index evaluating the water and thermal characteristics of proton exchange membrane fuel cell. Energy Convers. Manage. 185, 496–507.
Wang, Q., Zhou, Z.-Y., Lai, Y.-J., You, Y., Liu, J.-G., Wu, X.-L., Terefe, E., Chen, C., Song, L., Rauf, M., Tian, N., Sun, S.-G., 2014. Phenylenediamine-based FeNx/C catalyst with high activity for oxygen reduction in acid medium and its active-site probing. J. Am. Chem. Soc. 136, 10882–10885.
Wikipedia, 2015. Fuel cell vehicle.
Wilkinson, D.P., Lamont, G.J., Voss, H.H., Schwab, C., 1996. Embossed fluid flow field plate for electrochemical fuel cells, US.
William, D.E., 1999. PEM-Type fuel cell assembly having multiple par-allel fuel cell sub-stack employing shared fluid plate assembles andshared membrane electrode assemblies, US.
Wu, H., Li, X., Berg, P., 2009. On the modeling of water transport in polymer electrolyte membrane fuel cells. Electrochim. Acta 54, 6913–6927.
Yahya, M.S., Ismail, M., 2018. Synergistic catalytic effect of $SrTiO_3$ and Ni on the hydrogen storage properties of $MgH_2$. Int. J. Hydrogen Energy 43, 6244–6255.
Yang, H.-J., Cho, Y., Yoo, S.-H., 2017. Public willingness to pay for hydrogen stations expansion policy in Korea: Results of a contingent valuation survey. Int. J. Hydrogen Energy 42, 10739–10746.
Yoshiake, E., 1999. Solid polymer electrolyte fuel cell, US.
Zhang, G., Jiao, K., 2018. Multi-phase models for water and thermal management of proton exchange membrane fuel cell: A review. J. Power Sources 391, 120–133.
Zhang, S., Yuan, X.-Z., Hin, J.N.C., Wang, H., Friedrich, K.A., Schulze, M., 2009. A review of platinum-based catalyst layer degradation in proton exchange membrane fuel cells. J. Power Sources 194, 588–600.
Zhao, Y., 2013. Preparation of Mesoporous Silica and Its Applications in Hydrogen Storage Materials. City University of New York, Ann Arbor, p. 154.
Zhao, X., Li, Y., Liu, Z., Li, Q., Chen, W., 2015. Thermal management system modeling of a water-cooled proton exchange membrane fuel cell. Int. J. Hydrogen Energy 40, 3048–3056.
Zhao, Q., Majsztrik, P., Benziger, J., 2011. Diffusion and interfacial transport of water in Nafion. J. Phys. Chem. B 115, 2717–2727.
Zheng, Y., Chang, H., Chen, J., Chen, H., Shu, S., 2019. Effect of microgravity on flow boiling heat transfer of liquid hydrogen in transportation pipes. Int. J. Hydrogen Energy 44, 5543–5550.